Adverse effects of potassium on NO_x reduction over Di-Air catalyst (Rh/La-Ce-Zr)

Wang, Yixiao; Makkee, Michiel

DOI
10.1016/j.apcatb.2019.117895

Publication date
2019

Document Version
Accepted author manuscript

Published in
Applied Catalysis B: Environmental

Adverse effects of Potassium on NO_x reduction over Di-Air catalyst (Rh/La-Ce-Zr)

Yixiao Wang, Michiel Makkee

Catalysis Engineering,

Chemical Engineering Department,

Delft University of Technology,

Van der Maasweg 9,

2629 HZ Delft, The Netherlands.

Corresponding author:

m.makkee@tudelft.nl

Abstract

The influence of potassium in Rh on a lanthium promoted zirconia stablised ceria (CZ) catalysts was studied toward NO_x reduction reactivity and selectivity. The results are compared with a Rh/CZ catalyst. The samples were characterised by N_2 adsorption, XRD, SEM, ICP, and H_2-TPR. The study highlighted the importance of stored NO_x regeneration over potassium in determining the overall performance of the Rh/K/CZ catalyst. The NO_x stored over Rh/K/CZ in the previous NO gas stream cannot be regenerated sufficiently during the C_3H_6 gas stream, and stored NO_x gradually decreased from one cycle to the next, resulting in deteriorating performance of Rh/K/CZ. Besides, problem of NO_x slip, the formation of both NH_3 and N_2O (selectivities up to 30 % for each side product) were observed by the addition of potassium into the Rh/CZ catalyst system, depending on the reaction conditions applied and the severity of the catalyst deactivation.

Keywords: NO_x reduction, ceria, Rh, potassium, Di-Air

1. **Introduction**

Recently, the car manufactures and catalyst company are struggling to lower the NO_x emission. Unfortunately, the on-road real NO_x emissions are much higher than those are allowed under the Europe 6 emission regulation driving legislation [1-3]. Ammonia/ Urea-SCR is a mature technology to reduce NO_x emission from stationary sources and heavy-duty vehicles [4-6]. Although NH_3 (or urea) is an efficient reducing agent, the requirement for an injection system and NH_3 slip problem affect the economics and practicability of this application to passenger car, especially under the dynamic driving conditions. NO_x Storage and Reduction (NSR) system [7-9], developed by Toyota researchers, is regarded as the leading technology to control NO_x emission under lean-burn conditions. The engine is operating in the order of 60 seconds under the excess of oxygen (lean) condition. Subsequently, small hydrocarbon pulses are (in the order of 3 to 5 seconds) injected into the engine to create short periods with a reducing (rich) condition. Many challenges have still to be resolved. Firstly, the NO_x conversion decreases at high gas-flow conditions and at high temperatures. Secondly, during the lean and rich cycle switching step, the NO_x slip problem (up to 30 % slip of the stored NO_x) is highly unwanted. Thirdly, the formation of side products N_2O (very strong greenhouse gas) and NH_3 (toxicity) are of a major environmental concern. Most importantly, in the studies on the NSR catalyst using even most active reductant (H_2), the results showed that although at a relatively low temperature, the NO_x storage capacity was sufficient, but that the rates of NO_x release and reduction (NO_x conversion into nitrogen) were slow and insufficient, respectively [10, 11]. These drawbacks of the NSR technology will limit its application in the real driving, especially as of September 2017 in Europe. The European Commission had proclaimed that the real driving

emission (RDE) test protocol will partially replace the current certification laboratory test [12].

The application of the RDE requires that the catalyst has to work in wide temperature window and with a high space velocity (short contact time). Alternatives to the NO_x Storage Reduction and Ammonia (urea)-SCR systems, Di-Air system, Diesel NO_x after treatment by Adsorbed Intermediate Reductants, is under development, which is promising technology to efficiently abate NO_x especially at high temperatures and high flows all of the time in a lean burn exhaust gas stream. In this Di-Air system, continuously short fuel injections with a high frequency are applied downstream of the engine in the exhaust system upstream of a NSR catalyst ($Pt/Rh/Ba/K/Ce/Al_2O_3$) [13]. Limited information and experience are reported in both the open literature and patents archives on this newly developed technology. Mechanistic studies, especially on the Individual role of each catalyst component in the Di-Air system, are required to develop to reduce more deeply NO_x emissions from lean-burn gasoline and diesel vehicles and can come in compliance with the current and future more stringent NO_x emission standards.

In our previous work, the catalyst containing noble metal, especially Rh, and ceria are the promising starting materials for the Di-Air system. Ceria was found to be an critical catalyst ingredient in the Di-Air system. During the fuel injection, the oxygen from the ceria lattice can react with the fuel, resulting in several layers of ceria support reduction and a carbon deposition on the ceria surface [14]. The oxygen defects of ceria were found to be the key sites for the NO reduction into N_2 [15]. The deposited carbon formed during the fuel injection, acted as a buffer reductant. The oxidation of the deposited carbon will occur via the oxygen from the ceria lattice, which created additional oxygen vacancies for additional NO reduction. The loading of noble metals

over the ceria, *e.g.* Rh and Pt, can efficiently lower the ceria support reduction temperature by the fuel [16]. Additionally, the presence of noble metal will accelerate the N_2 formation rate. More importantly, the reduction of NO over a reduced Rh or Pt loaded ceria showed that NO was still selectively reduced into N_2 in an excess of oxygen (a factor of 100 in respect to NO, which is a typical value for a diesel engine exhaust stream) [17].

In the Di-Air system by Toyota, potassium (K) is one of the ingredients of the catalyst composition. Potassium (and/or barium) is a common ingredient in NSR catalyst, acting as the NO_x storage component during the fuel lean stage of the engine operation. The stored NO_x will be released and react with reductants from and during the fuel rich stage [18]. However, the reduction of the stored NO_x over potassium or barium is somewhat restricted or a kind of bottleneck for the entire NO_x storage and reduction process. NO_x storage sites are not completely regenerated during the fuel rich stage if the temperature was below 400 °C [19, 20]. Furthermore, the amount of NO_x released relatively to the amount stored decreased with decreasing temperatures, which can be determined by the relative rate of reductant production (from the fuel injection), nitrate decomposition, OSC (oxygen storage capacity) consumption, and actual NO_x reduction over the noble metal site of the NSR catalyst [20].

For a further optimisation the overall catalyst formulation and improving the performance of the Di-Air catalysts, it is meaningful to clarify whether potassium is required to add in the catalyst composition. Can the addition of potassium into Di-Air catalyst influence on the NO_x reduction performance, especially in NO_x slip, N_2O and NH_3 formation, and the deactivation on catalyst performance, which were so far not observed in the simplified Di-Air system of only a Rh and ceria based catalyst composition. To answer these questions, the NO reduction experiments on a ceria and

Rh ceria based catalyst with the addition of potassium with simulated exhaust gases were performed. Controlled experiment without potassium loading was included into the experiment approach.

2. **Experimental**

2.1. Materials preparation

Rh/CZ was prepared *via* an incipient wetness impregnation method of a rhodium precursor on Zr-La doped ceria (denoted as CZ, a gift from Engelhard, now BASF). Rhodium (III) nitrate hydrate (Aldrich, ~36% rhodium (Rh) basis) was used as the precursor. Subsequently, the sample was dried at 110 °C overnight and calcined at 550 °C for 5 h. For Rh/K/CZ, potassium was loaded on Rh/CZ by using incipient wetness impregnation method with $KHCO_3$ (Aldrich) as precursor, Subsequently, the sample was dried at 110 °C overnight and calcined at 550 °C for 5 h in a static air furnace.

2.2. Characterisation

2.2.1. Inductively Coupled Plasma Optical Emission Spectroscopy (ICP-OES)

Approximately 50 mg of sample was destructed in 4.5 ml 30% HCl + 1.5 ml 65% HNO_3 using the microwave. The destruction time in the microwave was 120 min at max power of 900 W. After destruction, the samples were diluted to 50 ml with MQ water. The samples were analysed with ICP-OES (PerkinElmer Optima 5300).

2.2.2. N_2 adsorption

Tristar II 3020 Micromeritics was used to determine the textural properties like specific BET surface area and pore volume. The catalyst samples were degassed at 200 °C for 16 h in a vacuum (0.05 mbar) before the nitrogen adsorption. The adsorption measurement was carried at -196 °C.

2.2.3. Scanning Electron Microscopy (SEM) and Energy-dispersive X-ray (EDX) Analysis

SEM images and EDX mapping of Rh/K/CZ was performed by using scanning electron microscope (JEOL JSM-6010 LA) equipped with an integrated EDX (Standard LA Version) with Silicon Drift Detector (SDD). The samples were analysed at accelerating voltage of 20 kV.

2.2.4. X-ray diffraction (XRD)

The Powder X-Ray diffraction (XRD) was recorded on a Bruker-AXS D5005 with a Co Kα source. The data were times collected by varying the 2θ angle from 30° to 90° with a step size of 0.02.

2.2.5. Temperature programming reaction (TPR)

TPR for all the samples were carried out in a fixed bed reactor system connected to a thermal conductivity detector (TCD) to monitor the consumption of hydrogen by the catalyst. 200mg of samples were packed between SiC layers (300 - 425 μm). The samples were then reduced in the H_2 (10 %)/Ar flow at a flow rate of 30 ml_{STP} min^{-1},

with temperature from room temperature to 1000 ◦C with a heating rate of 5 ◦C / min. TCD was calibrated by using CuO as a reference. A perma-pure tubular drier was used to remove the water produced during the reduction upstream of the TCD detector.

2.3. Catalytic Testing

2.3.1. Reactivity and selectivity study in flow reactor

A flow reactor was explored for the study of the NO reduction reactivity and selectivity with and without gas-phase oxygen. 200 mg catalyst was placed in a 6 mm inner-diameter quartz reactor tube. The reactor effluent was online analysed by a mass spectrometry (MS, Hiden Analytical, HPR-20 QIC) and infrared (IR) spectroscopy (Perkin–Elmer, Spectrum One). For the IR analysis a gas cell with KBr windows with a path length of ~5 cm was used. The spectra were measured in a continuous mode using the Perkin-Elmer 'Time-Base' software between 4000 - 700 cm^{-1} wavenumbers with a spectral resolution of 8 cm^{-1} and an acquisition of 8 scans per spectrum, resulting in a time interval of 23 s between each displayed spectrum. For the NO reduction in the presence of O_2, a feed composition of 0.2% NO and 5 % of O_2 (with He as balance) was used with a space velocity of 67.0000 L/L/h. Prior to the feeding in 0.2% NO and 5% O_2 in He, the catalyst was firstly pre-treated by 1.25% C_3H_6 in He for 2 h. **Scheme 1** described the experiment procedural.

Scheme 1

2.3.2. He-Temperature Programmed Desorption (TPD) after NO and O_2 co-adsorption

200 mg catalyst was placed inside a quartz tube. The reactor effluent was online analysed by infrared (IR) spectroscopy (Perkin–Elmer, Spectrum One). Prior to Temperature Programmed Desorption experiments, the sample was firstly oxidised at 600 ◦C with 5% O_2 in He in order to remove carbon residues, *e.g.* adsorbed CO_2. Subsequently, the samples were exposed to the reactive gas ((2000 ppm NO + 5 % O_2)/He balance) at 200 °C for 10 h. Afterward, the samples were outgassed in He in order to remove the weakly bound physical adsorbed NO_x. After cooling down to 40 ◦C, the samples were heated up from 40 to 700 ◦C with a heating rate of 5 ◦C / min using He as the carrier gas (200 mL / min). Concentration profiles of NO, N_2O, and NO_2 in parts per million (ppm) were obtained. The IR spectrometer was calibrated with 1% NO, 1% N_2O, and (1% NO_2 + 2 % O_2) in He, respectively.

2.3.3. *In-situ* Drift

Infrared spectra were recorded in the 4000−700 cm^{-1} range (resolution = 8 cm^{-1}, 128 scans), performed by a Thermo Scientific Nicolet 8700 FT-IR spectrometer using MCT detector with a KBr beam splitter. The catalyst was placed in the cell and the gas was flown through the catalyst bed (30 $ml_{STP}\,min^{-1}$), confined in a three-window chamber.

2.3.4. Temporal Analysis of Products (TAP) study

H_2 and C_3H_6 titration experiments were performed in TAP over a pre-oxidised and pre-nitrated Rh/K/CZ to reduce oxidised and nitrated Rh/K/CZ, respectively. Pre-oxidised Rh/K/CZ was exposed to about 2000 pulse of 80 vol. % O_2 in Ar, and pre-nitrated

sample was exposed to about 2000 pulse of 80 vol. % ^{15}NO in Kr. Rh/K/CZ reduction experiments were performed by using either 66.7 vol. % H_2 in Ar or 80 vol. % C_3H_6 in Ne both at 450 ˚C.

The NO reduction was performed using 80 vol.% ^{15}NO in Kr over Rh/CZ and Rh/K/CZ. H_2 was used to pre-reduce the samples until H_2 and H_2O MS signals were stable. Subsequently, ^{15}NO was pulsed.

10 mg Rh/CZ and Rh/K/CZ were investigated in the TAP reactor. In all experiments starting pulse sizes of approximately $2 \cdot 10^{15}$ molecules, including reactants (80 vol. %) and inert gas (20 vol. %), were used. The inert gas was used as internal standard. The pulse size gradually decreased during an experiment since as the reactant was pulsed from a closed and calibrated volume of the pulse-valve line. Details can be found elsewhere [15].

3. **Results**

3.1. Characterisation

Figure 1. SEM-EDX analysis of fresh Rh/K/CZ.

Characterisation details of the Zr-La doped ceria support (hereafter denoted as CZ) were reported elsewhere [15, 21]. In brief, a typical fluorite structure of CZ was detected by Raman and XRD. The crystal size of CZ determined by the Scherrer's equation and TEM image analyses was 5.0 nm for both techniques. The BET surface area was 65 m^2/g. The BET surface area of fresh and used Rh/CZ and Rh/K/CZ were

similar to the bare CZ support (65±2 m^2/g). Measured by the ICP-OES, the loading of Rh was determined to be 0.5 wt % for the samples of Rh/CZ and Rh/K/CZ. The particle size of Rh was around 2 nm from TEM [17]. The loading of K was determined to be 5 wt % for the samples of K/CZ and Rh/K/CZ. **Figure 1** shows the SEM and EDX mapping images of Rh/K/CZ. The intensities in EDX signal were represented as the colour code on the left scale. As shown in Figure 1, Zr, La, and Ce were all homogeneously distributed. K was highly homogenous dispersed with a few numbers of small agglomerates. Rh could not be detected due to its low loading (0.5 wt %).

Figure 2

Table 1

Figure 2A shows the XRD patterns of oxidised CZ, Rh/CZ, and Rh/K/CZ. The patterns of metal loaded samples showed the fluorite cubic structure of the CZ. Diffraction lines to be assigned to Rh and K metals or any their oxides could not be observed. The reduction properties of Rh/K/CZ, Rh/CZ, and CZ were studied by TPR-H_2 technique, as presented in **Figure 2B**. The pure ceria generally showed two-peak pattern due to surface and bulk reduction at the temperature of 500 and 750 ˚C, respectively [22]. The bare CZ sample showed a main broad reduction feature with roughly two peaks at 430 and 550 ˚C. The lower temperature reduction peak as compared to the pure ceria might be due to the promotion of the reduction in the bulk of the mixed oxide upon doping with ZrO_2 [23]. Compared to bare CZ support, surface and bulk reduction of Rh/CZ

shifted to lower temperatures. For the Rh/K/CZ with a potassium loading of 5 % potassium, the feature of low-temperature H_2 reduction disappeared while the higher-temperature H_2 reduction peak slightly shifted to a lower temperature in comparison to the Rh/CZ sample, but at the same time the consumption of hydrogen almost doubled. The amount of H_2 consumption is reported in **Table 1**.

3.2. Catalytic testing

3.2.1. NO reduction in the absence of O_2 in fixed bed reactor

Figure 3

Figure 3 shows the results of exposure 0.2 % NO/He over the C_3H_6 reduced Rh/CZ at 450 ˚C with a GHSV of 67.000 L/L/h. **Figure 3A** shows the MS response of gasses from the exit of the reactor. m/e = 28 was observed, attributed to the formation of N_2 and CO. NO was not observed during the first 460 s. A low intensity of m/e = 44 was observed, attributed to the formation of CO_2. Figure 3B shows the FT-IR spectra of the gasses from the exit of the reactor. Peaks at 2174 and 2116 cm^{-1}, attributed to CO, were observed instantly when switching to the NO gas stream. The CO peak intensity increased to the maximum at the time of 250 s and then declining. Hardly any CO formation was observed after 1500 s. A low intensity of peak at 2350 cm^{-1}, assigned to CO_2, was also observed during the first 500 s. 1908 and 1850 cm^{-1} were observed from 460 s onwards, assigned to NO. The rise of two bands at 1601 and 1628 cm^{-1} from 1500 s onwards was attributed to the formation of NO_2. Small peaks at 2235 and 2208

cm^{-1}, assigned to N_2O, were only observed after 460 s, which was from the impurity in the NO gas bottle at the level of 1 ppm. The NO reduction experiments were recycled 4 times over the same Rh/CZ sample, as described in **Scheme 1**. The results could be repeated. The NO conversion showed the same reactivity regardless to the number of NO cycles experiment.

Figure 4

The same experiments were performed over the sample containing potassium. **Figure 4** shows the results of the exposure of 0.2 % NO/He over the fresh Rh/K/CZ pre-treated by C_3H_6 at 450 ˚C with GHSV of 67.000 L/L/h. **Figure 4A** shows the MS response of the gasses from the exit of the reactor. Similar to the result over Rh/CZ, m/e = 28 was observed, attributed to the formation of N_2 and CO. The CO formation was confirmed by FT-IR peaks at 2174 and 2116 cm^{-1} (**Figure 4B**). From **Figure 4C**, the highest CO concentration was less than 500 ppm. Small amount of CO_2 formation was observed from the FT-IR spectra. No NO was observed during the first 750 s, followed by NO signal intensity gradually increased. The N_2O band, centred at 2235 and 2208 cm^{-1}, started to appear from the time of 500 s, arriving at a maximum level of 25 ppm (**Figure 4C**).

Figure 5

The NO reduction experiments were additionally performed over the used Rh/K/CZ, in which the Rh/K/CZ was firstly pre-adsorbed NO during the 1st NO reduction experiment and then pre-treated by C_3H_6 during the 2nd cycle experiment, as described in **Scheme 1**. During the 2nd run of the NO experiment, NO started to form from t = 500 s. The NO signal increasing rate during the 2nd run of NO experiment was much steeper than that during the 1st run (**Figure 4C and 5B**). N_2O formation was observed instantly when switching over to the NO gas stream. The highest CO concentration was around 50 ppm, which was less than that during the 1st run, as shown in **Figure 4C**. During the 4th NO reduction experiment, NO started to be observed from the time of 475 s onwards. The NO signal increasing rate during the 4th run of NO experiment is similar to that during the 2nd run (**Figure 4C and 5B**). N_2O was observed instantly upon NO exposure.

3.2.2. NO reduction in the presence of O_2 in fixed bed reactor

Figure 6

Figure 6A shows the MS response during (0.2 % NO+ 5 % O_2)/He over the C_3H_6 reduced Rh/CZ at 400 ◦C. Full NO conversion was observed during the first 69 s, followed by a gradual decreasing in the NO conversion. Both m/e = 28 and m/e = 44 were observed from the t = 0 s and their intensities dropped down from t = 23 s. The observation of m/e = 28 was attributed to the formation of N_2 and CO. Both CO_2 and N_2O could contribute to the MS response at m/e = 44. O_2 started to breakthrough after 5 s and became stable after 10 s.

From the FT-IR (**Figure 6B**), CO and CO_2 were formed from the start of the NO flow and reached maximum production at the time of 23 s, afterwards the CO formation dropped down. N_2O was not observed during the first 69 s. 1 ppm N_2O was observed after 69 s, which came from the impurity of the NO gas bottle. Therefore, the MS response of m/e = 44 was assigned to the formation of CO_2. The concentrations of NO, NO_2, N_2O, CO, and CO_2 during the (0.2 % NO + 5% O_2)/He gas stream gas stream were plotted and shown in **Figure 6C**. NO an NO_2 started to breakthrough almost at the same time (t = 69 s) and they became stable after 250 s, and hardly any CO_2 was observed.

The results of NO reduction experiments over C_3H_6 reduced Rh/CZ were repeated during at least 4 cycles of NO experiment. The complete NO conversion time interval remained the same during the 4 cycles of NO reduction experiment, as shown in **Figure 6D**.

Figure 7.

The NO reductions in the presence of O_2 were additionally performed over the fresh propene pre-reduced Rh/K/CZ and used propene reduced and followed by a NO/O_2 pre-treated Rh/K/CZ. **Figure 7** shows the MS response during (0.2 % NO+ 5% O_2)/He as stream over the C_3H_6 reduced Rh/K/CZ at 400 °C for the 1st run of NO experiment over fresh Rh/K/CZ. As illustrated in **Figure 7A**, O_2 was broken through instantly (t = 0 s) and it became stable from time of 15 s. NO showed a period of full conversion (around 340 s). From 340 s onwards, a progressive increasing of NO was observed. m/e = 28 was observed with high intensity up to 20 s, followed by a low intensity till t =

70 s. The observed m/e = 28 was assigned to CO and N_2. Similarly, a high intensity of m/e = 44 was observed up to 20 s. A constant intensity of m/e = 44 was observed between t = 20-340 s, followed by gradual decline till the end of the experiment. The observed m/e = 44 was assigned to CO_2 and N_2O.

Figure 7B shows the results of the 4th cycle of NO experiment. Low intensities of m/e = 28 and m/e = 44 were observed. NO showed a shorter time interval for full conversion (around 70 s) as compared to the 1st cycle of NO experiment (340 s). From 70 s onwards, a breakthrough of NO signal was observed in MS. O_2 broke through instantly (time of 0 s) and became stable at 5 s.

Figure 8

Figure 8 shows the FT-IR spectra during (0.2 % NO + 5% O_2)/He gas stream. For the 1st cycle of NO reduction experiment (**Figure 8A**), Peak at 2350 cm^{-1}, assigned to CO_2, was observed from the beginning of (0.2 % NO + 5 % O_2)/He gas stream. Similarly, peaks at 2174 and 2116 cm^{-1}, attributed to CO, were observed instantly during the (0.2 % NO + 5 % O_2)/He gas stream. Both CO and CO_2 intensity declined from the time of t = 23 s onwards. Peaks at 1908 and 1850 cm^{-1} were observed from 340 s onwards and was assigned to NO. The rise of two bands at 1601 and 1628 cm^{-1} from 600 s was attributed to the formation of NO_2. N_2O, centring at 2235 and 2208 cm^{-1}, was observed during whole (0.2 % NO + 5 % O_2)/He gas stream exposure. **Figure 8B** shows the FT-IR results of the 4th cycle of NO reduction experiment. As compared to **Figure 8A**, less CO_2 and CO were formed during the (0.2 % NO + 5 % O_2)/He gas

stream. In addition, NO and NO_2 started to rise from the time of 77 s and 200 s, respectively, in the 4th cycles.

Figure 9

Figure 9 shows the NO (Figure 9A) and NO_2 (Figure 9B) breakthrough time during (0.2 % NO + 5 % O_2)/He gas stream. The full NO conversion time interval dropped from 340 s at 1st NO run to 45 s at 6th NO experiment cycle. The formation of NO_2 started from 600 s at 1st NO run experiment, and started from 140 s at 6th NO experiment. The formation of NO_2 appeared earlier when increasing the cycles.

3.2.3. NO_x-TPD and *in-situ* DRIFTS

Figure 10

The NO_x-TPD experiments were carried out over the Rh/CZ and Rh/K/CZ. **Figure 10A** shows the result of NO_x-TPD in He. For Rh/CZ, two NO_x desorption regions were observed, centred at 250 and 400 ◦C, respectively. No NO_x desorption were observed after 450 ◦C. For Rh/K/CZ, a wide NO_x desorption temperature range was observed, especially, significant amount of NO_x desorption was observed above 600 ◦C.

The chemical structure and stability of adsorbed NO_x species were studied by *in-situ* DRIFTS. A DRIFT spectrum was firstly recorded in Ar after 30 min of reaction in the ^{15}NO/Ar gas mixture. The reaction feed stream was then switched to a C_3H_6/Ar gas mixture and DRIFT spectra were continuously recorded. **Figure 10B** shows the recorded spectra. The pre-nitrated Rh/K/CZ sample showed peaks at 1341, 1212, and 1542 cm^{-1}. The IR bands centered at 1542 cm^{-1} corresponded to the *v* NO_2(as), *v* NO_2(sym), and *v* N-O vibrational modes of bidentate nitrate formed on the Rh/K/CZ. The band at 1212 cm^{-1} could be assigned to asymmetric (v_{as}) and symmetric (v_{sym}) NO stretching mode of the chelating nitrite (NO_2^-). The band at 1434 cm^{-1} was assigned to adsorbed *nitrosyl* (NO_2^+). The assignments of the various adsorbed NO_x species were based on well-documented literature data [24]. When switching to the C_3H_6/Ar gas stream, the band at 1212 cm^{-1} vanished after 9 min, accomplishing with three new peaks at the position of 2143, 1971 cm^{-1}, and 1420. The peak at 1420 cm^{-1} was assigned to the carbonate [25]. The peak at 1542 cm^{-1} remained constant while the peak at 1341 cm^{-1} slightly decreased. The peaks at 2143 and 1971 cm^{-1} did not show up over the Rh/CZ sample, as shown in **Figure 10D**. In order to identify the species of the peaks at 2143 and 1971 cm^{-1}, an isotope switching experiment were performed. The experimental protocol was shown in the **Figure 10C**. Over the fresh Rh/K/CZ sample in air, only carbonate species were observed in the region of 1420 cm^{-1}. When switching to ^{14}NO/Ar gas, peaks at the position of 1542, 1341, and 1222 cm^{-1} were observed, which were assigned to bidentate nitrate, *nitrosyl* , and chelating nitrite. The peaks at 2160 and 2036 cm^{-1} were observed during C_3H_6/Ar gas stream while they disappeared when switching to ^{15}NO/Ar gas stream. Chelating nitrite ($^{15}NO_2^-$), peak at 1212 cm^{-1}, was observed during ^{15}NO/Ar gas stream, which disappeared when switching to C_3H_6/Ar. Peaks at 2143 and 1971 cm^{-1} were appeared, which were the

same species as peaks at 2160 and 2036 cm^{-1} due to the isotope shift. Neither the peaks at 2160 and 2036 cm^{-1} nor at 2143 and 1971 cm^{-1} were not observed during the H_2 gas stream over pre-nitrated Rh/K/CZ. Therefore, the peaks of 2143 and 1971 cm^{-1} (2160 and 2036 cm^{-1}) were confirmed containing N and C, which could be assigned to the surface CNO or NC species [26, 27].

3.2.4. H_2 and C_3H_6 pulses over pre-oxidised and ^{15}NO pre-nitrated Rh/K/CZ samples in TAP

Figure 11A shows the results of the H_2 pulse over the pre-oxidised fresh Rh/K/CZ sample at 400 ˚C. The pulse of H_2 led to the H_2O formation. H_2 experienced full conversion and started to breakthrough after pulse number 300. For the pre-nitrated Rh/K/CZ, as shown in **Figure 11B**, the pulse of H_2 firstly led to the formation of NO, H_2O, and $^{15}NH_3$. The N_2 formation started from pulse number 100 and disappeared at pulse number 400. H_2 did not show a full conversion from the beginning of H_2 pulse. The H_2 conversion increased from pulse number 100 till full conversion at the pulse number of 300, subsequently, its conversion gradually declined.

Figure 11

Figure 12

.

The reduction of ^{15}NO pre-nitrated Rh/K/CZ was also performed by pulsing C_3H_6. As shown in **Figure 12**, C_3H_6 showed 50 % conversion at the beginning of the C_3H_6 pulse, followed by a C_3H_6 conversion increase to 100 % conversion at pulse number 40. C_3H_6 showed full conversion between pulse number 40 and 200, followed by a C_3H_6 conversion decline. $^{15}N_2$, H_2O, and $^{15}NH_3$ were formed during the first 100 C_3H_6 pulses. ^{15}NO and $^{15}N_2$ formation diminished at the end of 100 C_3H_6 pulses and subsequently the C_3H_6 oxidation reaction led to the formation of CO_2, CO, and H_2.

3.2.5. $^{15}N_2$ response comparison during ^{15}NO pulse over H_2 reduced Rh/CZ and Rh/K/CZ

Figure 13A shows the $^{15}N_2$ response during the first 90 ^{15}NO pulses over H_2 pre-reduced fresh Rh/K/CZ, where all the NO was converted, *i.e.,* NO signal did not have a response. The $^{15}N_2$ showed a sharp response at the first ^{15}NO pulse; then, the response became broader with the intensity decreasing during the subsequent ^{15}NO pulses. Additionally, the N_2 peak was at t = 0.056 s during the 1st ^{15}NO injection, and the peak shifted to t = 0.126 s at the 90th ^{15}NO injection. $^{15}N_2$ peak shifted to a later time during NO pulse sequence, indicating the slower and slower $^{15}N_2$ formation rate with ^{15}NO pulses. The pulses of ^{15}NO would lead to the Rh/K/CZ was nitrated. After the ^{15}NO pulses, C_3H_6 was used as a reductant to reduce the nitrated Rh/K/CZ. Both Figures 13B and C show the $^{15}N_2$ responses during the ^{15}NO pulses over a C_3H_6 pre-reduced nitrated Rh/K/CZ sample at the 2nd and 3rd ^{15}NO pulsing cycles, respectively. Both Figure 13B and C show that the N_2 response became broader with pulse number, indicating that $^{15}N_2$ formation rate became slower and slower. In contrast, over the

Rh/CZ sample, $^{15}N_2$ responses hardly changed during the ^{15}NO pulses as the indicated ^{15}NO pulses number.

Figure 13

4. **Discussion**

Potassium (or barium) is a common ingredient in NSR catalyst, acting as the NO_x storage component during the fuel-lean stage of the engine operation. The general problems of NSR technology are narrow operating temperature window, low space velocity, N_2O formation, NH_3 formation, and NO_x slip. The problems are mainly caused by the NO_x storage and release materials. The Di-Air system showed a broader operating temperature window (up to 800 ^oC) and higher space velocity (up to 120.000 L/L/h), where the storage component hardly can have a role in the NO_x reduction. From our previous work, we have found that the oxygen anion vacancies in ceria are responsible for the decomposition of NO into N_2, thereby, re-oxidising these defect centres. The delayed oxidation of the carbon deposits by the oxygen species originating from the lattice oxygen will in practice maintain a reduced surface state of the ceria during the fuel-lean conditions. These carbon deposits (created from the fuel injection), therefore, can be seen as a stored reductant with a delayed (buffer) function. The loading of Rh (noble metal) is mainly to lower the fuel activation temperature, to lower the ceria support reduction temperature, and to accelerate N_2 formation rate. Although potassium and barium are ingredients in the Di-Air catalyst composition, it is necessary to investigate the role of these NO_x storage materials. What will be the exact role of these components and what will be the consequence by the addition. The

discussion will be focused on the comparison between catalysts with and without potassium loading from the perspectives of catalyst performance stability, NO slip, NH_3- and N_2O- formation and in the end the effectiveness of the NO conversion into the selectivity of the N_2 formation.

4.1. The effect of potassium on the stability of catalyst performance

C_3H_6 was used to reduce the catalyst to mimic the consequence of fuel injection in the Di-Air system [14]. The Rh lowered the C_3H_6 oxidation temperature over the CZ [14]. At the temperature below 450 ◦C, the reduction of CZ support was not favoured [14]. By loading Rh, the reduction of CZ by C_3H_6 at 450 ◦C was obtained around 3 hypothetical reduced CZ layers with additional carbon deposition.

The reactivity of NO reduction was investigated in a flow reactor under atmospheric pressure. Prior to the NO reduction experiments, 1.25% C_3H_6/He was used to pre-treat the Rh/K/CZ and Rh/CZ at 450 ◦C for 2 h before each cycle of NO experiments, as shown in the experimental scheme (**Scheme 1**). The pre-treatment by C_3H_6 led to the reduction of CZ support and deposition of carbon on the catalyst surface [16]. The H_2-TPR experiment (Figure 2B) showed significant changes in reduction peak position between Rh/CZ and Rh/K/CZ. Therefore, the addition of potassium hardly changed the lattice oxygen reactivity. The amount of H_2 consumption over Rh/K/CZ was almost two times of that over Rh/CZ. For K-containing NSR catalyst, several kinds of K species can be existed in the form of K_2O, KOH, and K_2CO_3 [28]. The K_2CO_3 could be reduced to CO_2 and H_2O at lower temperature, around 200 ◦C, initiated by surface hydroxyl groups [29, 30].Therefore, separately from the contribution of the reduction of CZ support, the H_2 consumption was accounted for the the reduction of surface carbonate.

The results of **Figure 3A** showed the reduction of NO into N_2 over the C_3H_6 pre-reduced Rh/CZ. The FT-IR spectra (**Figure 3B**) confirmed the formation of CO and CO_2 and excluded the formation of NO_2 and N_2O during the first 460 s, where NO was completely converted. The conversion of NO into N_2 was confirmed by the ^{15}NO experiment, as reported in our previous work [17].

The oxygen vacancies were the catalytic sites for the NO reduction into N_2. The reduction of NO resulted in a re-oxidation of the reduced Rh/ CZ. Subsequently, the oxygen from the (re-oxidised) CZ lattice was further reacted with the deposited carbon to form CO and CO_2, thus additional oxygen vacancies were created and the new oxygen vacancies were used for additional NO reduction. NO appeared in the exit exhaust stream after 460 s. In the time frame from 450 s till 1500 s the rest of carbon deposited was oxidised. From 1500 s onwards NO was partially converted into NO_2. As shown in **Figure 3D**, the complete NO conversion time interval remained the same during the 4 cycles and indicated the high stability of Rh/CZ sample during the C_3H_6 pre-treatment and NO reduction process.

In the presence of potassium the overall product evolution profile for the C_3H_6 reduced Rh/K/CZ catalyst during the NO reduction was similar to that of Rh/CZ over fresh sample. This was due to the oxygen vacancies playing a role in NO reduction. The NO, however, started to break through at t =750 s (Figure 4), which was 290 s longer than the NO over Rh/CZ. The extended duration of the NO conversion was due to the presence of potassium, which could adsorb additional NO as potassium nitrite and nitrate [31]. The difference between the fresh and the used Rh/K/CZ was significant. The NO breakthrough time dropped from 750 s for the 1^{st} cycle to 450 s for the 4^{th} cycle (Figure 5). Potassium was common ingredient in the NSR system to store NO_x during the fuel lean stage.

For the Rh/K/CZ catalyst the fresh and pre-nitrated surface affected the C_3H_6 reactivity. Apparently, less CO was formed during the NO gas stream over the used Rh/K/CZ sample (**Figure 4 and 5**). The less CO formation indicated the low reactivity of C_3H_6 for a recycled 'potassium' catalyst. The BET surface of Rh/K/CZ before and after the reaction remained similar, therefore, the reactivity difference between the fresh and used Rh/K/CZ was ascribed to the nitrate or nitrite formation. The formation of nitrate or nitrite was confirmed by the *in-situ* Drift as shown in Figure 10B. A long NO admission time led to nitrites and slowly transformation into nitrates. The formation of nitrate and nitrite species stabilised the CZ lattice oxygen reducibility, which caused to a low C_3H_6 reactivity. The addition of alkali metals into V_2O_5/CeO_2 catalysts led also to the deactivation for the selective catalytic reduction of NO_x with NH_3 in the SCR reaction. Potassium decreased the surface acidity and lowered the reducibility of the ceria and V_2O_5, both suppressing the NH_3 adsorption and NH_3 activity for the SCR reaction [32]. Therefore, the addition of potassium into the Rh/CZ system will lower the C_3H_6 reactivity by the stabilisation of the ceria lattice oxygen.

In our TAP study, different reductant reactivity's over pre-oxidised and pre-nitrated Rh/K/CZ were observed. The pulsing of even the most active reductant, H_2, showed different reactivity over the fresh and pre-nitrated Rh/K/CZ samples. H_2 showed a full conversion to H_2O over the oxidised Rh/K/CZ sample, but around 80% conversion over the the pre-nitrated sample (**Figure 11**). The presence of nitrate/nitrite inhibited the CZ support reduction reactivity.

In the presence of gas-phase oxygen, NO transformed in nitrate-like species over the potassium sample [33]. At the temperature of 450 ˚C, a stronger stability of nitrate species in the form of polydentate species was formed [34]. The formation of such stable species during a long NO exposure inhibited the reaction between C_3H_6 and

Rh/CZ. As shown in **Figure 9**, the NO started to breakthrough from 45 s at the 4th cycle experiment, as compared to 340 s at the 1st cycle experiment. Additionally, the NO_2 breakthrough time dropped. With the cycles of ($NO+O_2$) experiments, the NO adsorption on the potassium led to a more stable polydentate nitrate species that deteriorated the reversible NO_x storage capacity. More importantly, unlike the Rh/K/CZ, the NO breakthrough for Rh/CZ remained the same time during the whole NO experiment cycles (69 s), as shown in **Figure 6D**. The difference behaviours in the NO breakthrough time (**Figure 6D and Figure 9**) indicated clearly that the potassium was the component for the deactivation of Rh/K/CZ in NO reactivity in cycles of NO reduction experiment. To validate this conclusion, the stability of stored NO_x over Rh/K/CZ was studied both by NO_x-TPD in He (**Figure 10A**) and under reductant gas stream (**Figure 10B and 10C**). The NO_x-TPD showed that a broad temperature window of NO_x desorption till 700 ◦C. The desorbed NO_x up to 380 ◦C was likely related to the decomposition of nitrites, whereas those desorption species above 380˚C were more related to the desorption of nitrates [35]. During this temperature ramp, the nitrite species also transformed into the nitrate species. Apparently, significant amount of the adsorbed NO_x was strongly adhesive to the Rh/K/CZ, which required temperature above 700 ◦C to completely regenerate the catalyst to be free of adsorbed NO_x. Additionally, *in-situ* Drift experiments were performed to investigate the thermal stability of adsorbed NO_x in the presence of reductant. As shown in **Figure 10B**, the exposure of pre-nitrated Rh/K/CZ under C_3H_6 environment led to the formation of peaks at 2143 and 1971 cm^{-1}, which was further confirmed in **Figure 10C** that these two peaks contained both N and C atoms. During the C_3H_6 exposure, only the chelating nitrite peaks disappeared. The *in-situ* Drift experiments demonstrated that C_3H_6 was

not able to completely regenerate the N storage over the surface at the temperature of 450 ˚C.

H_2 and CO were regarded to have a relatively high nitrate reduction efficiency compared to that of C_3H_6 and C_3H_8 [36]. In the Di-Air system, fuel was used as reductant and was directly injected over the catalyst. The reaction between C_3H_6 and pre-nitrated Rh/K/CZ showed similar reaction step. As shown in **Figure 12**, the pulses of C_3H_6 firstly led to the formation of H_2O, $^{15}NH_3$, $^{15}N_2$, and ^{15}NO. The formation of CO_2 was secondly followed by the formation of H_2 and CO from pulse number of 90 indicated the participation of CZ lattice oxygen in C_3H_6 complete reaction and cracking reaction. Therefore, C_3H_6 needed to react with the adsorbed nitrite and nitrate species before the CZ lattice oxygen could participate in the C_3H_6 reaction. The low reactivity of hydrocarbon towards the nitrate(s) would eventually affect the life time of the catalyst.

4.2. The effect on potassium on the NH_3 formation and NO slip

Regarding the ammonia formation, ammonia evolution occurred after introducing the H_2 and hydrocarbons over the NSR catalyst. The formation of ammonia could act as reductant to reduce NO_x into N_2, especially for the SCR reaction of NO_x with NH_3. It was well-known that both the NO_x slip and NH_3 formation were main hurdles to the tackle in the NSR system. Therefore, a combined NSR (upstream) and SCR (downstream) $DeNO_x$ system was developed, aiming to solve the NH_3 and NO_x challenges [37].

The pulsing of H_2 over a ^{15}NO pre-nitrated Rh/K/CZ led to an initial reaction between H_2 and surface nitrate/nitrite with formation of H_2O, $^{15}NH_3$, $^{15}N_2$, and ^{15}NO (F**igure 11B**). The $^{15}N_2$ and ^{15}NO formation diminished after the pulse number 400. The reduction of

CZ support led to the water formation after pulse number 400. Therefore, the reduction of pre-nitrate Rh/K/CZ by H_2 firstly led to the reduction of surface absorbed nitrite and subsequently to the CZ support reduction. The formation of ammonia depended on the local coverage of chemisorbed N and H atoms [38]. The introduction of H_2 initially led to the NO_x slip that was due to the fast NO_x desorption at the temperature of 450 ˚C. The formation of ammonia favoured when the NO_x desorption rate dropped down (from pulse number 80 to 800) and the concentration of surface H species increased. In our TAP experiment, the introduction of H_2 firstly led to the $^{15}NH_3$ formation and some NO slip. The reduction of NO_x into N_2 started from pulse number 80. $^{15}N_2$ was formed during the pulse number 80 to 400, which could be due to the decomposition of NO_x over the reduced site of Rh/K/CZ or the reduction of NO_x by the formed ammonia. Similarly, the introduction of C_3H_6 over the pre-nitrated Rh/K/CZ also led to the ^{15}NO slip and $^{15}NH_3$ formation (**Figure 12**).

4.3. The effect of potassium on the N_2O formation and N_2 formation rate

N_2O formation has a large impact the NO reduction over a NSR catalyst. In our study, N_2O formation was only observed over the potassium containing samples.

For Rh/CZ, during the full NO conversion time interval (t = 0 - 460 s), neither N_2O and NO_2 was formed (**Figure 3**). The observation of m/e = 28 indicated the reduction of NO into N_2. Even 1 ppm N_2O coming from the impurity in of NO gas bottle was reduced. Therefore, a reduced ceria, acting as '*oxygen black hole'* [16], selectively reduced NO and traces of N_2O into N_2.

When the Rh/CZ was reduced, most probably associated with an oxygen vacancy linked to a Ce^{3+} cation. The adsorption of NO over the reduced site of Ce led to NO

dissociation, as described in equation (1), and recombination of N_{ads} into N_2, as described in equation (2).

$$NO + Ce^{3+} \rightarrow Ce^{4+} - O + N_{ads} \quad \text{(equation 1)}$$

$$N_{ads} + N_{ads} \rightarrow N_2 \quad \text{(equation 2)}$$

Reading the N_2O formation during the NO reduction process, two steps were proposed for the formation of N_2O over Pt and Rh in the literature [39]:

$$NO + 2NM \rightarrow NM - N + NM - O \quad \text{(step 1, equation 3)}$$

$$NM - N + NO \rightarrow N_2O + NM \quad \text{(step 2, equation 4)}$$

Over the Rh/CeO_2-ZrO_2 system hardly any N_2O formation was observed [40]. In the presence of noble metal, the combination of N_{ads} into N_2 step was faster than the reaction between NO and N_{ads}.

For the fresh Rh/K/CZ, a level of 25 ppm of N_2O was, however, observed from t = 500 s, where a full NO conversion was observed (**Figurer 4**). Over the used Rh/K/CZ sample, N_2O was instantly formed during the NO exposure (**Figure 5**). When an excess of oxygen vacancies was available over the nitrate free Rh/K/CZ catalyst, *e.g.,* t < 500 s in **Figure 4**, NO was selectively reduced into N_2 and no N_2O was observed. The decreasing of the CO formation from t = 400 s onwards indicated the depletion of the deposited carbon over the Rh/K/CZ sample and the largely (re-)oxidised of CZ support. N_2O started to be formed, when CO intensity largely decreased, *i.e.,* N_2O was formed over a less reduced Rh/K/CZ sample. This hypothesis/observation was in line with the observation over the used Rh/K/CZ sample, as shown in **Figure 5**. The difference between the fresh and used Rh/K/CZ sample was the adsorption of NO_x over the K on the used Rh/K/CZ, which had a significant influence on the C_3H_6 reactivity

and the CZ support reduction, as described in section 4.1. To sum up, the addition of potassium into the CZ catalyst clearly led to a significant N_2O formation.

For a NSR catalyst, the stored NO_x over potassium or barium component was supposed to be converted into N_2, but N_2O was commonly observed. N_2O was both formed during the lean/rich switching transient. The formation of N_2O during the fuel rich conditions was attributed to either the incomplete reduced catalyst sites or the reaction between reductants and intermediates. While the N_2O formation during the rich to lean switching originated from the oxidation of the reduction intermediates remaining on the surface, which included adsorbed ammonia, NH_4NO_3, or isocyanates. In our experimental protocol, lean/rich switching transients were not really existed and the N_2O formation was also not only observed during the switching of reaction conditions. Therefore, the formation of N_2O could not completely be attributed to the decomposition of ammonia, NH_4NO_3, or isocyanates.

Different reaction rates of NO dissociation and N_{ads} combination into N_2 might explain the N_2O formation by the addition of potassium to Rh/CZ catalyst, as shown in equation 1-4. N_2O can be formed *via* recombination of NO, adsorption over the surface, and with N, left over the surface. Therefore, the relative reaction rate among the N recombination into N_2, surface concentration of NO, and NO dissociation rate are critical to the N_2O formation. In order to understand the process of the NO reduction over the potassium containing sample, NO pulses experiments over a H_2 reduced Rh/CZ and Rh/K/CZ were performed. The N_2 response during the ^{15}NO pulses can provide information on the NO reduction process.

The results of TAP experiment by pulsing ^{15}NO over a H_2 reduced Rh/CZ showed that a fast N species (re)combination into N_2. There was hardly N-species left over the

Rh/CZ surface during each NO injection. However, the injection of ^{15}NO over a H_2 reduced Rh/K/CZ led to a slower N_2 formation rate as compared to that over the Rh/CZ sample (**Figure 13**). The N_2 formation slowed down during the ^{15}NO pulses. Since no ^{15}NO was observed by the MS during the ^{15}NO injection, the slower N_2 formation rate was due to slow N-species (re)combination process. Therefore, when the reaction was performed under the atmosphere pressure and under high space velocity, the adsorbed N-species combined with the NO to form N_2O over the potassium containing catalyst.

5. **Conclusions**

To summarise the addition of potassium into the Rh/CZ catalyst deteriorated performance of the catalysts. Over a clean Rh/K/CZ catalyst, the initial NO conversion performance, including the NO reduction and strorage, was determined both by the rate of NO_x storage capacity and the oxygen vacancies capacity. The NO_x stored over Rh/K/CZ in the previous lean phase could not be regenerated sufficiently upon C_3H_6 exposure and the levels of stored (unreduced) NO_x gradually increased from one cycle to the next, resulting in deteriorating performance of the potassium containing catalysts. Besides, the well-known problems of NO_x slip and NH_3 formation over the NSR the addtion of potassium led to the N_2O formation and slowed down the reaction rate of N_{ads} combination into N_2. It is, therefore, recommended for an efficient Di-Air NO_x abatement technology to avoid the addition of potassium to the noble metal ceria (Rh/CZ) catalyst system.

Acknowledgement

The authors acknowledge the China Scholarship Council (CSC) for their financial support.

6. References

[1] D.C. Carslaw, S.D. Beevers, J.E. Tate, E.J. Westmoreland, M.L. Williams, Recent evidence concerning higher NO_x emissions from passenger cars and light duty vehicles, Atmospheric Environment, 45 (2011) 7053-7063.

[2] L. Yang, S. Zhang, Y. Wu, Q. Chen, T. Niu, X. Huang, S. Zhang, L. Zhang, Y. Zhou, J. Hao, Evaluating real-world CO_2 and NO_X emissions for public transit buses using a remote wireless on-board diagnostic (OBD) approach, Environmental Pollution, 218 (2016) 453-462.

[3] F.P.S. Vicente Franco, John German, and Peter Mock, REAL-WORLD EXHAUST EMISSIONS FROM MODERN DIESEL CARS, (2014).

[4] M. Koebel, M. Elsener, T. Marti, NOx-reduction in diesel exhaust gas with urea and selective catalytic reduction, Combustion science and technology, 121 (1996) 85-102.

[5] W.R. Miller, J.T. Klein, R. Mueller, W. Doelling, J. Zuerbig, The development of urea-SCR technology for US heavy duty trucks, in, SAE Technical Paper, 2000.

[6] H. Hug, A. Mayer, A. Hartenstein, Off-highway exhaust gas after-treatment: Combining urea-SCR, oxidation catalysis and traps, in, SAE Technical Paper, 1993.

[7] S.i. Matsumoto, Recent advances in automobile exhaust catalyst, Catalysis Surveys from Asia, 1 (1997) 111-117.

[8] Y. Ikeda, K. Sobue, S. Tsuji, S.i. Matsumoto, Development of NO_x Storage-Reduction Three-way Catalyst for D-4 Engines, in, SAE Technical Paper, 1999.

[9] M. Misono, T. Inui, New catalytic technologies in Japan, Catal. Today, 51 (1999) 369-375.

[10] Y. Sakamoto, T. Motohiro, S. Matsunaga, K. Okumura, T. Kayama, K. Yamazaki, T. Tanaka, Y. Kizaki, N. Takahashi, H. Shinjoh, Transient analysis of the release and reduction of NO_x using a $Pt/Ba/Al_2O_3$ catalyst, Catalysis Today, 121 (2007) 217-225.

[11] J. Sjöblom, K. Papadakis, D. Creaser, C.I. Odenbrand, Use of experimental design in development of a catalyst system, Catalysis today, 100 (2005) 243-248.

[12] http://europa.eu/rapid/press-release_MEMO-17-2821_en.htm.

[13] Y. Bisaiji, K. Yoshida, M. Inoue, K. Umemoto, T. Fukuma, Development of Di-Air-A New Diesel $deNO_x$ System by Adsorbed Intermediate Reductants, SAE International Journal of Fuels and Lubricants, 5 (2012) 380-388.

[14] Y. Wang, M. Makkee, Fundamental understanding of the Di-Air system (an alternative NO_x abatement technology):(I) the difference in reductant pre-treatment of ceria, Applied Catalysis B: Environmental, 223 (2018) 125-133.

[15] Y. Wang, J. Posthuma de Boer, F. Kapteijn, M. Makkee, Next Generation Automotive $DeNO_x$ Catalysts: Ceria What Else?, ChemCatChem, 8 (2016) 102-105.

[16] Y. Wang, R. Oord, D. van den Berg, B.M. Weckhuysen, M. Makkee, Oxygen Vacancies in Reduced Rh/ and Pt/Ceria for Highly Selective and Reactive Reduction of NO into N_2 in excess of O_2, ChemCatChem, 9 (2017) 2935-2938.

[17] Y. Wang, F. Kapteijn, M. Makkee, NO_x reduction in the Di-Air system over noble metal promoted ceria, Applied Catalysis B: Environmental, 231 (2018) 200-212.

[18] W.S. Epling, L.E. Campbell, A. Yezerets, N.W. Currier, J.E. Parks, Overview of the fundamental reactions and degradation mechanisms of NO_x storage/reduction catalysts, Catalysis Reviews, 46 (2004) 163-245.

[19] N. Takahashi, K. Yamazaki, H. Sobukawa, H. Shinjoh, The low-temperature performance of NO_x storage and reduction catalyst, Applied Catalysis B: Environmental, 70 (2007) 198-204.

[20] W.S. Epling, A. Yezerets, N.W. Currier, The effects of regeneration conditions on NO_x and NH_3 release from NO_x storage/reduction catalysts, Applied Catalysis B: Environmental, 74 (2007) 117-129.

[21] Y. Wang, J.P. Boer, F. Kapteijn, M. Makkee, Fundamental Understanding of the Di-Air System: The Role of Ceria in NO_x Abatement, Topics in Catalysis, 59 (2016) 854-860.

[22] H.C. Yao, Y.F.Y. Yao, Ceria in automotive exhaust catalysts: I. Oxygen storage, Journal of Catalysis, 86 (1984) 254-265.

[23] M. Daturi, E. Finocchio, C. Binet, J.-C. Lavalley, F. Fally, V. Perrichon, H. Vidal, N. Hickey, J. Kašpar, Reduction of High Surface Area CeO_2−ZrO_2 Mixed Oxides, The Journal of Physical Chemistry B, 104 (2000) 9186-9194.

[24] C.M. Kalamaras, G.G. Olympiou, V.I. Pârvulescu, B. Cojocaru, A.M. Efstathiou, Selective catalytic reduction of NO by H_2/C_3H_6 over $Pt/Ce_{1-x}Zr_xO_{2-\delta}$: The synergy effect studied by transient techniques, Applied Catalysis B: Environmental, 206 (2017) 308-318.

[25] G.N. Vayssilov, M. Mihaylov, P.S. Petkov, K.I. Hadjiivanov, K.M. Neyman, Reassignment of the vibrational spectra of carbonates, formates, and related surface species on ceria: a combined density functional and infrared spectroscopy investigation, The Journal of Physical Chemistry C, 115 (2011) 23435-23454.

[26] V. Matsouka, M. Konsolakis, R.M. Lambert, I.V. Yentekakis, In situ DRIFTS study of the effect of structure (CeO_2-La_2O_3) and surface (Na) modifiers on the catalytic and surface behaviour of Pt/γ-Al_2O_3 catalyst under simulated exhaust conditions, Applied Catalysis B: Environmental, 84 (2008) 715-722.

[27] N. Bion, J. Saussey, M. Haneda, M. Daturi, Study by in situ FTIR spectroscopy of the SCR of NO_x by ethanol on Ag/Al_2O_3-Evidence of the role of isocyanate species, Journal of Catalysis, 217 (2003) 47-58.

[28] N. Hou, Y. Zhang, M. Meng, Carbonate-based lean-burn NO_x trap catalysts $Pt–K_2CO_3/ZrO_2$ with large NO_x storage capacity and high reduction efficiency, The Journal of Physical Chemistry C, 117 (2013) 4089-4097.

[29] A. Iordan, M.I. Zaki, C. Kappenstein, C. Géron, XPS and in situ IR spectroscopic studies of $CO/Rh/Al_2O_3$ and $CO/Rh/K–Al_2O_3$ at high temperatures: probing the impact of the potassium functionalization of the support, Physical Chemistry Chemical Physics, 5 (2003) 1708-1715.

[30] Z.-Q. Zou, M. Meng, J.-J. He, Surface distribution state and storage performance of the potassium species in the lean-burn NO_x trap catalyst $Pt/K/Al_2O_3–TiO_2–ZrO_2$, Materials Chemistry and Physics, 124 (2010) 987-993.

[31] I. Nova, L. Castoldi, L. Lietti, E. Tronconi, P. Forzatti, F. Prinetto, G. Ghiotti, NO_x adsorption study over Pt–Ba/alumina catalysts: FT-IR and pulse experiments, Journal of Catalysis, 222 (2004) 377-388.

[32] Y. Peng, J. Li, X. Huang, X. Li, W. Su, X. Sun, D. Wang, J. Hao, Deactivation Mechanism of Potassium on the V_2O_5/CeO_2 Catalysts for SCR Reaction: Acidity, Reducibility and Adsorbed-NO_x, Environmental Science & Technology, 48 (2014) 4515-4520.

[33] M. Symalla, A. Drochner, H. Vogel, S. Philipp, U. Göbel, W. Müller, IR-study of formation of nitrite and nitrate during NO_x-adsorption on NSR-catalysts-compounds CeO_2 and BaO/CeO_2, Topics in Catalysis, 42 (2007) 199-202.

[34] T. Montanari, L. Castoldi, L. Lietti, G. Busca, Basic catalysis and catalysis assisted by basicity: FT-IR and TPD characterization of potassium-doped alumina, Applied Catalysis A: General, 400 (2011) 61-69.

[35] K. Krishna, A. Bueno-López, M. Makkee, J.A. Moulijn, Potential rare-earth modified CeO_2 catalysts for soot oxidation part II: Characterisation and catalytic activity with $NO+O_2$, Applied Catalysis B: Environmental, 75 (2007) 201-209.

[36] S. Mulla, S. Chaugule, A. Yezerets, N. Currier, W. Delgass, F. Ribeiro, Regeneration mechanism of $Pt/BaO/Al_2O_3$ lean NO_x trap catalyst with H_2, Catalysis Today, 136 (2008) 136-145.

[37] F. Can, X. Courtois, S. Royer, G. Blanchard, S. Rousseau, D. Duprez, An overview of the production and use of ammonia in NSR+SCR coupled system for NO_x reduction from lean exhaust gas, Catalysis today, 197 (2012) 144-154.

[38] A. Kouakou, F. Dhainaut, P. Granger, F. Fresnet, I. Louis-Rose, Study of Ammonia Formation During the Purge of a Lean NO_x Trap, Topics in Catalysis, 52 (2009) 1734.

[39] B.K. Cho, B.H. Shank, J.E. Bailey, Kinetics of NO reduction by CO over supported rhodium catalysts: Isotopic cycling experiments, Journal of Catalysis, 115 (1989) 486-499.

[40] F. Fajardie, J.-F. Tempère, J.-M. Manoli, O. Touret, G. Blanchard, G. Djéga-Mariadassou, Activity of Rh^{x+} Species in CO Oxidation and NO Reduction in a $CO/NO/O_2$ Stoichiometric Mixture over a Rh/CeO_2-ZrO_2 Catalyst, Journal of Catalysis, 179 (1998) 469-476.

SCHEME

Scheme 1. Experimental protocol in the fixed bed reactor

TABLE

Table 1. H_2 consumption in TPR experiments for Rh/K/CZ, Rh/CZ, and CZ.

FIGURES

Figure 1. SEM-EDX analysis of fresh Rh/K/CZ.

Figure 2. (A) XRD patterns and (B) H_2-TPR of oxidised CZ, Rh/CZ, and Rh/K/CZ.

Figure 3. Gases evolution from the exit of the reactor: (A) MS signal; (B) FT-IR spectra; (C) the quantitative data from (B); and (D) complete NO conversion time interval *versus* the number of NO experiment cycles. All the experiments were performed at the condition of 0.2% NO/He gas stream over C_3H_6 reduced Rh/CZ at 450 ◦C , GHSV of 67.000 L/L/h.

Figure 4. Gases evolution from the exit of the reactor: (A) MS signal; (B) FT-IR spectra; (C) the quantitative data from (B). The experiments were performed at the condition of 0.2% NO/He gas stream over fresh Rh/K/CZ pre-treated by C_3H_6 at 450 ◦C, GHSV of 67.000 L/L/h.

Figure 5. Gases evolution from the exit of the reactor: (A) and (C) FT-IR spectra; (B) and (D) are the quantitative data from (A) and (C), respectively. (A) and (C) were obtained during the 2^{nd} and 4^{th} NO experiment, respectively. Both experiments were performed at the conditions of 0.2% NO /He gas stream over an used Rh/K/CZ pre-treated by C_3H_6 at 450 ◦C, GHSV of 67.000 L/L/h.

Figure 6. (A) MS signal, (B) FT-IR spectra; and (C) the concentration of gases during 0.2% NO + 5% O_2 in He flow over C_3H_6 reduced Rh/CZ at 400 ◦C; (D) total NO conversion time interval *versus* the number of NO cycles experiment.

Figure 7. Gasses evolution during exposure of Rh/K/CZ C_3H_6 reduced at 400 ◦C to a 0.2% NO + 5% O_2 containing He flow at a GHSV of 67.000 l/l/h at 400 ◦C. (A) 1^{st} cycle of NO and (B) 4^{th} cycle of NO experiments.

Figure 8. FT-IR response during (0.2 % NO + 5% O_2) exposure over at 400◦C C_3H_6 reduced Rh/K/CZ (A)1^{st} and (B) 4^{th} cycle of NO reduction experiements.

Figure 9. NO and NO_2 breakthough time *versus* the number of NO experiment cycles during (0.2 % NO + 5% O_2) exposure over C_3H_6 reduced Rh/K/CZ at 400°C.

Figure 10. (A) NO_x-TPD in He recorded after exposure to (0.5% NO + 5%O_2)/He at 200 °C over Rh/CZ and Rh/K/CZ, *in-situ* Drift spectra during C_3H_6/Ar over ^{15}NO pre-nitrated (B) Rh/K/CZ and (D) ^{15}NO Rh/CZ, (C) isotope gas switching experiment over Rh/K/CZ.

Figure 11. H_2 over NO pre-oxidised (A) and ^{15}NO pre-nitrated Rh/K/CZ at 450 °C, Ar was used as internal standard.

Figure 12. C_3H_6 over ^{15}NO pre-nitrated Rh/K/CZ at 450 °C, Ne was used as internal standard.

Figure 13. $^{15}N_2$ response during ^{15}NO pulses over (A) H_2 pre-reduced Rh/K/CZ (fresh), (B) C_3H_6 pre-reduced Rh/K/CZ (pre-nitrated, 2nd cycle), (C) C_3H_6 pre-reduced Rh/K/CZ (pre-nitrated, 3rd cycle), and (D) H_2 pre-reduced Rh/CZ (both used and fresh).

SCHEME

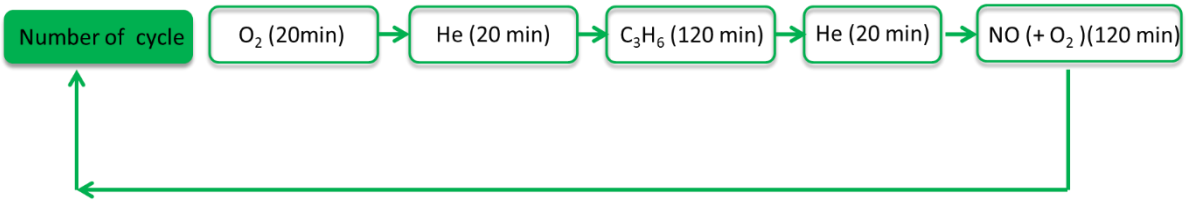

Scheme 1. Experimental protocol in the fixed bed reactor

TABLE

Sample	H_2 consumption (mmol/g_{cat})
CZ	1.2
Rh/CZ	1.7
Rh/K/CZ	2.7

Table 1. H_2 consumption in TPR experiments for Rh/K/CZ, Rh/CZ, and CZ.

FIGURES

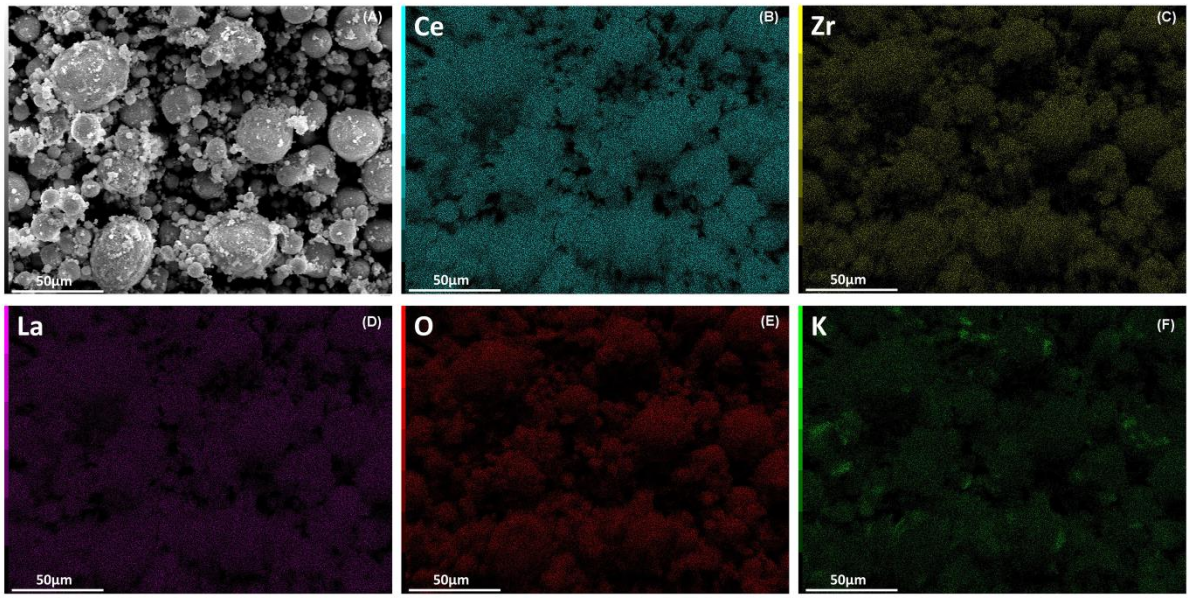

Figure 1. SEM-EDX analysis of fresh Rh/K/CZ.

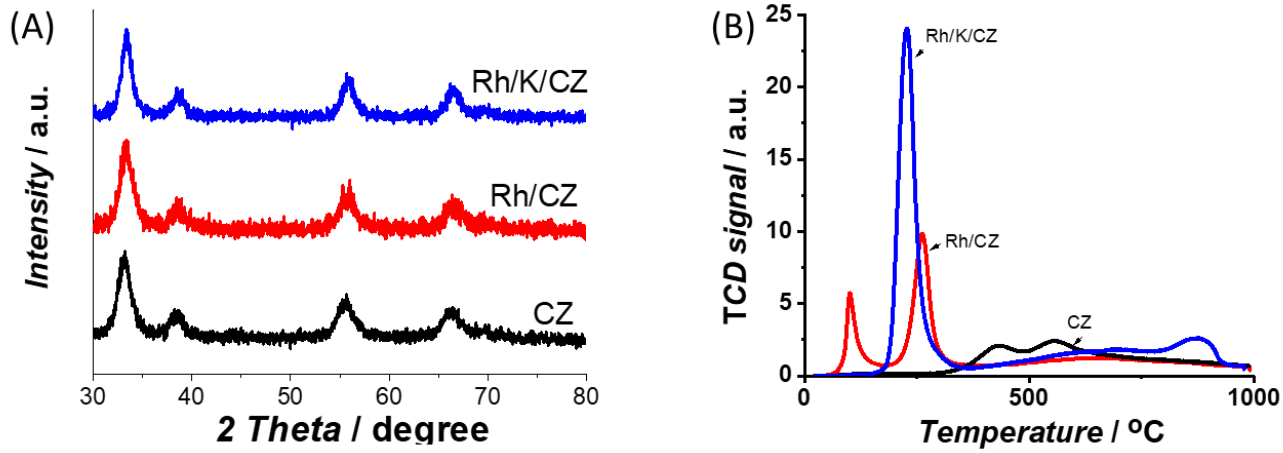

Figure 2. (A) XRD patterns and (B) H_2-TPR of oxidised CZ, Rh/CZ, and Rh/K/CZ.

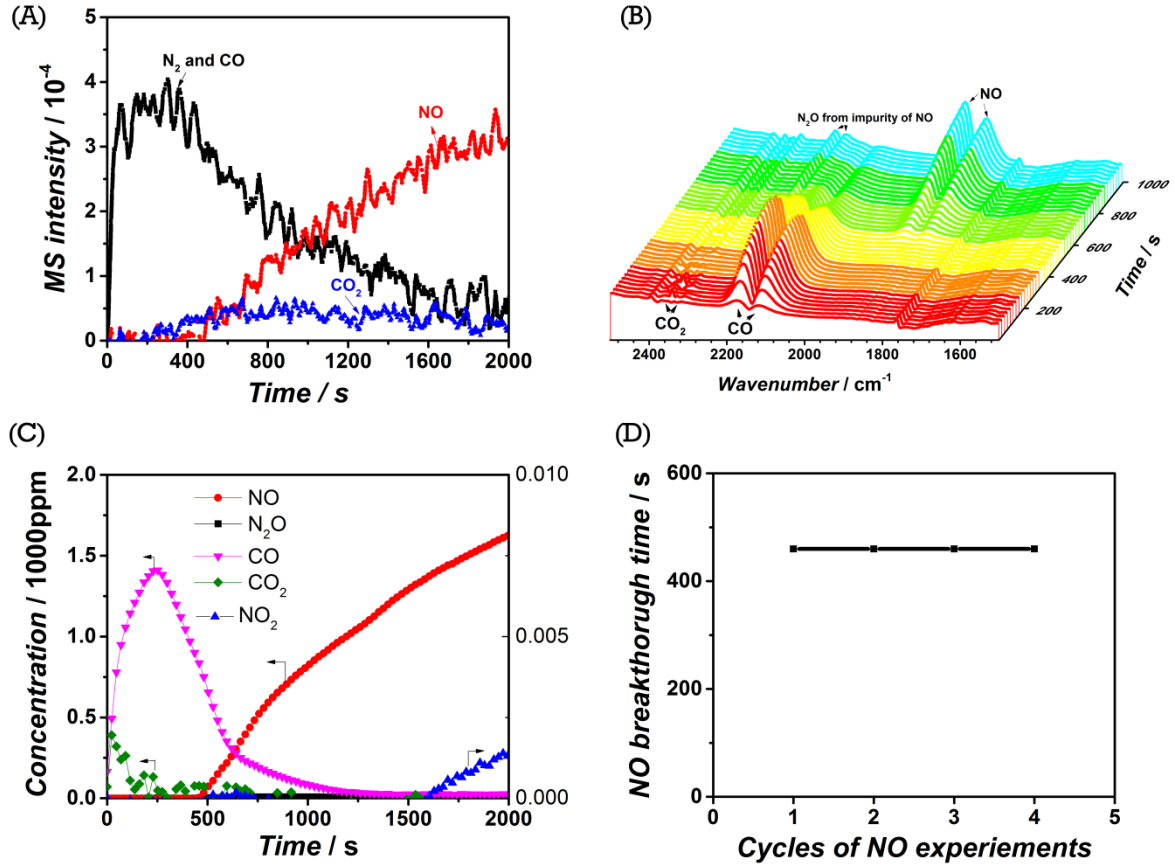

Figure 3. Gases evolution from the exit of the reactor: (A) MS signal; (B) FT-IR spectra; (C) the quantitative data from (B); and (D) complete NO conversion time interval *versus* the number of NO experiment cycles. All the experiments were performed at the condition of 0.2% NO/He gas stream over C_3H_6 reduced Rh/CZ at 450 ◦C, GHSV of 67.000 L/L/h.

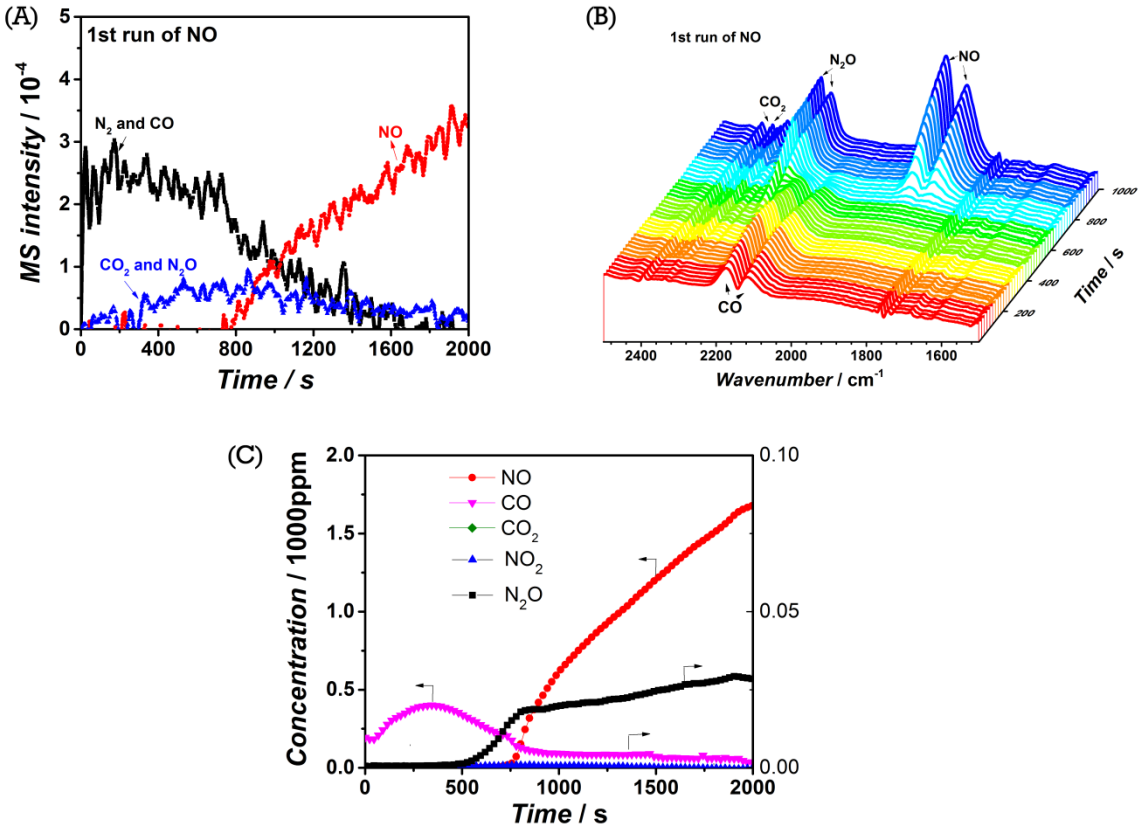

Figure 4. Gases evolution from the exit of the reactor: (A) MS signal; (B) FT-IR spectra; (C) the quantitative data from (B). The experiments were performed at the condition of 0.2% NO/He gas stream over fresh Rh/K/CZ pre-treated by C_3H_6 at 450 ◦C, GHSV of 67.000 L/L/h.

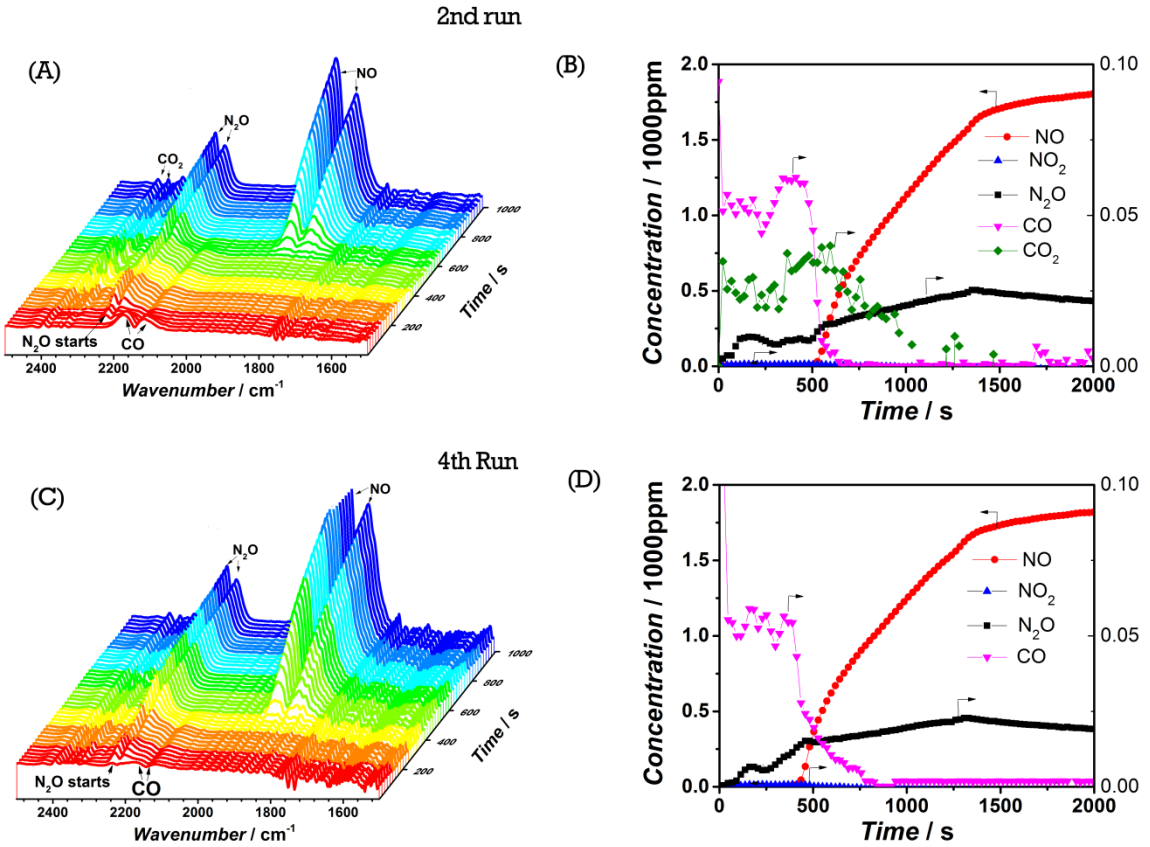

Figure 5. Gases evolution from the exit of the reactor: (A) and (C) FT-IR spectra; (B) and (D) are the quantitative data from (A) and (C), respectively. (A) and (C) were obtained during the 2nd and 4th NO experiment, respectively. Both experiments were performed at the conditions of 0.2% NO /He gas stream over an used Rh/K/CZ pre-treated by C_3H_6 at 450 °C, GHSV of 67.000 L/L/h.

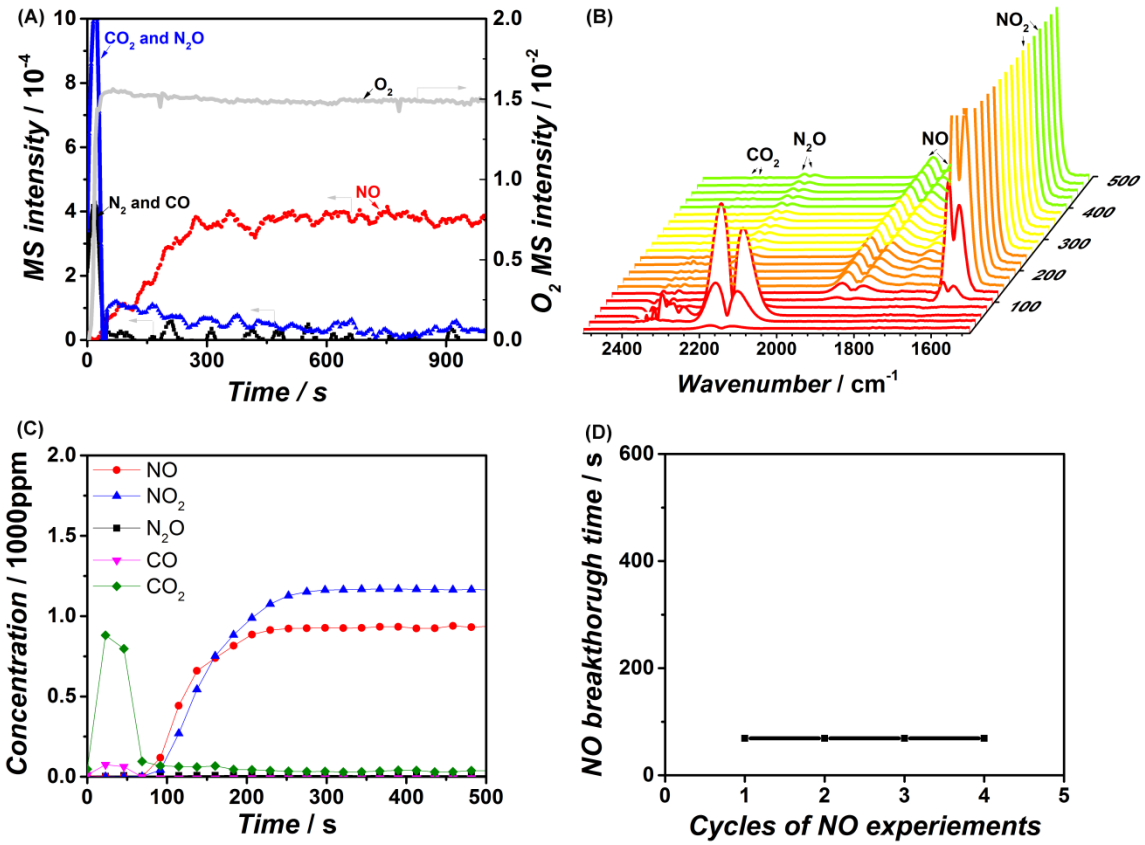

Figure 6. (A) MS signal, (B) FT-IR spectra; and (C) the concentration of gases during 0.2% NO + 5% O_2 in He flow over C_3H_6 reduced Rh/CZ at 400 ◦C; (D) total NO conversion time interval *versus* the number of NO cycles experiment

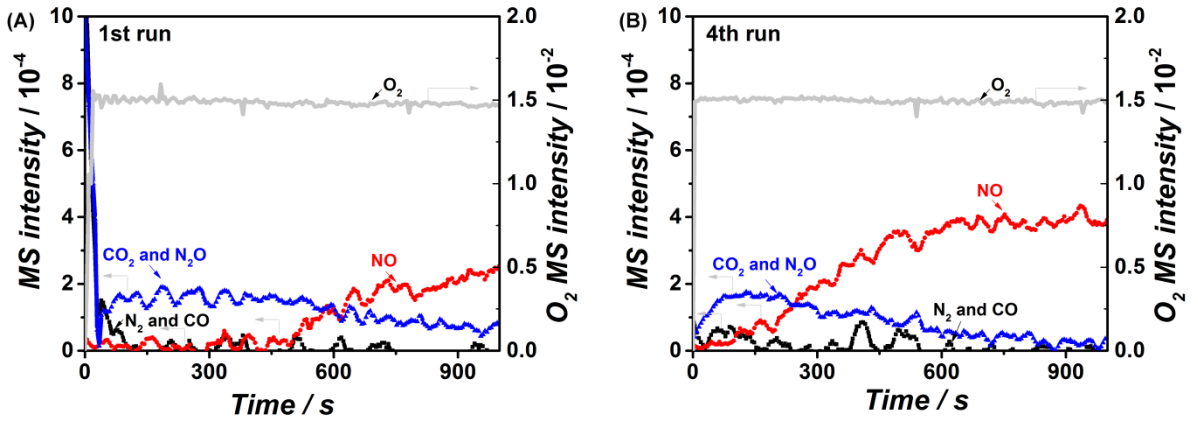

Figure 7. Gasses evolution during exposure of Rh/K/CZ C_3H_6 reduced at 400 ◦C to a 0.2% NO + 5% O_2 containing He flow at a GHSV of 67.000 l/l/h at 400 ◦C. (A) 1st cycle of NO and (B) 4th cycle of NO experiments.

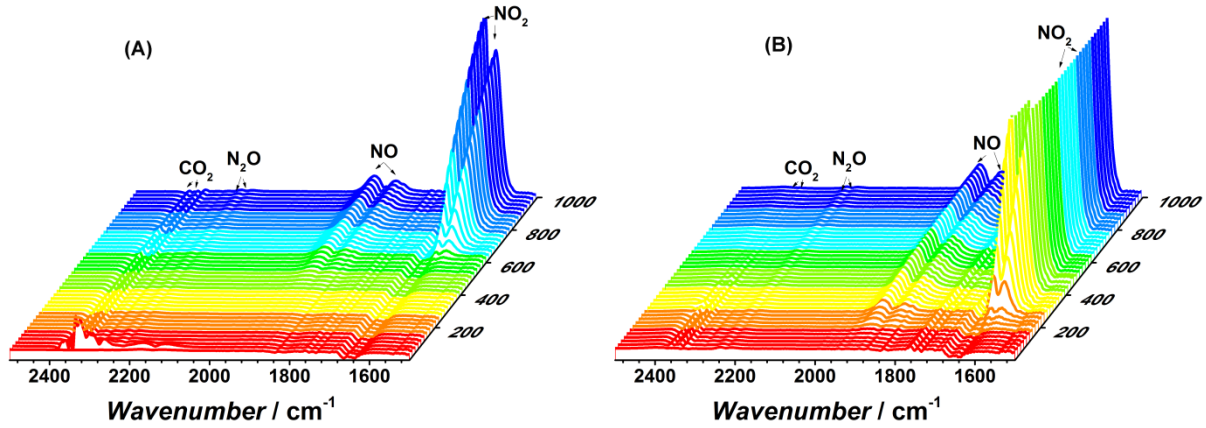

Figure 8. FT-IR response during (0.2 % NO + 5% O_2) exposure over at 400◦C C_3H_6 reduced Rh/K/CZ (A)1st and (B) 4th cycle of NO reduction experiements.

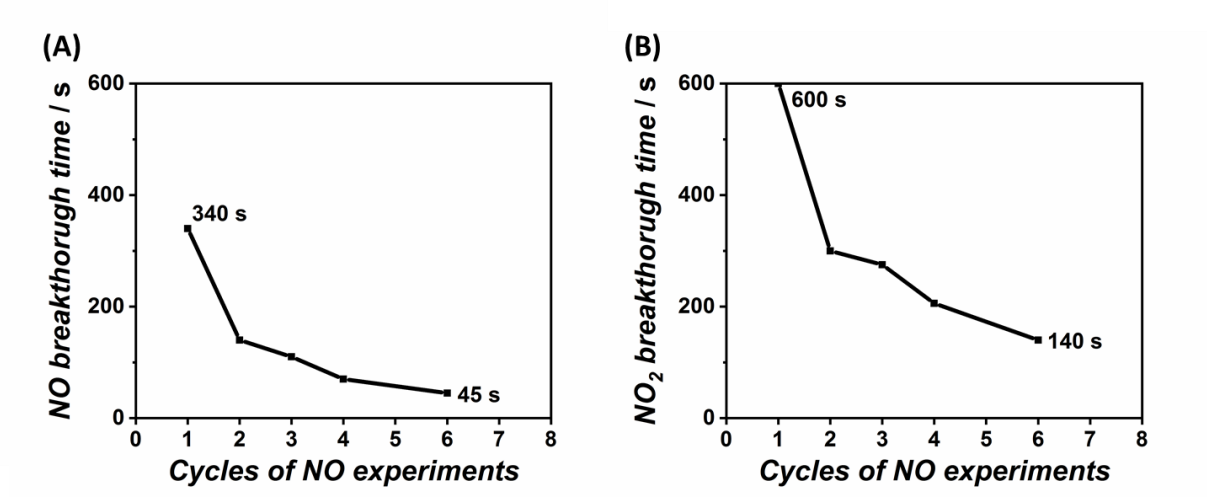

Figure 9. NO and NO_2 breakthough time *versus* the number of NO experiment cycles during (0.2 % NO + 5% O_2) exposure over C_3H_6 reduced Rh/K/CZ at 400°C.

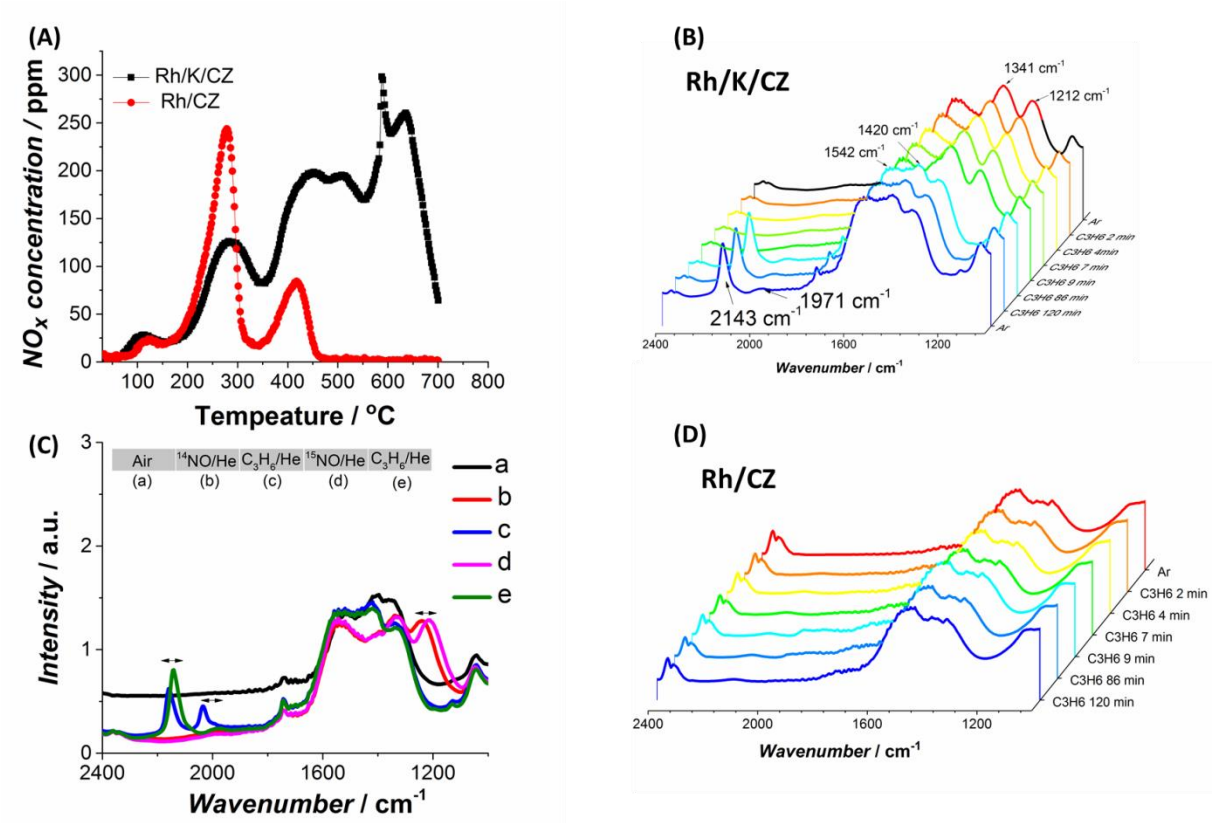

Figure 10. (A) NO_x-TPD in He recorded after exposure to (0.5% NO + 5%O_2)/He at 200 °C over Rh/CZ and Rh/K/CZ, *in-situ* Drift spectra during C_3H_6/Ar over ^{15}NO pre-nitrated (B) Rh/K/CZ and (D) ^{15}NO Rh/CZ, (C) isotope gas switching experiment over Rh/K/CZ.

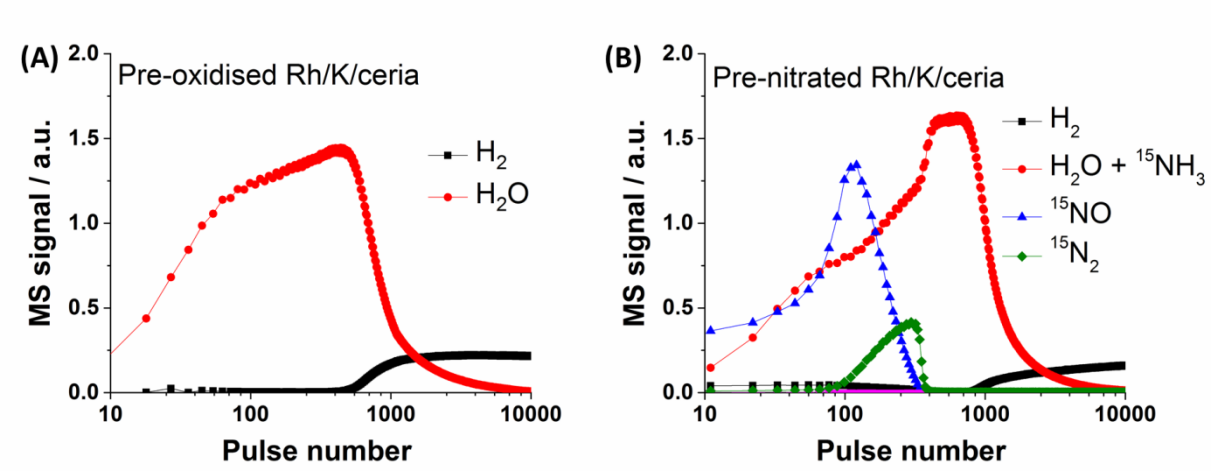

Figure 11: H_2 over NO pre-oxidised (A) and ^{15}NO pre-nitrated Rh/K/CZ at 450 ^{o}C, Ar was used as internal standard.

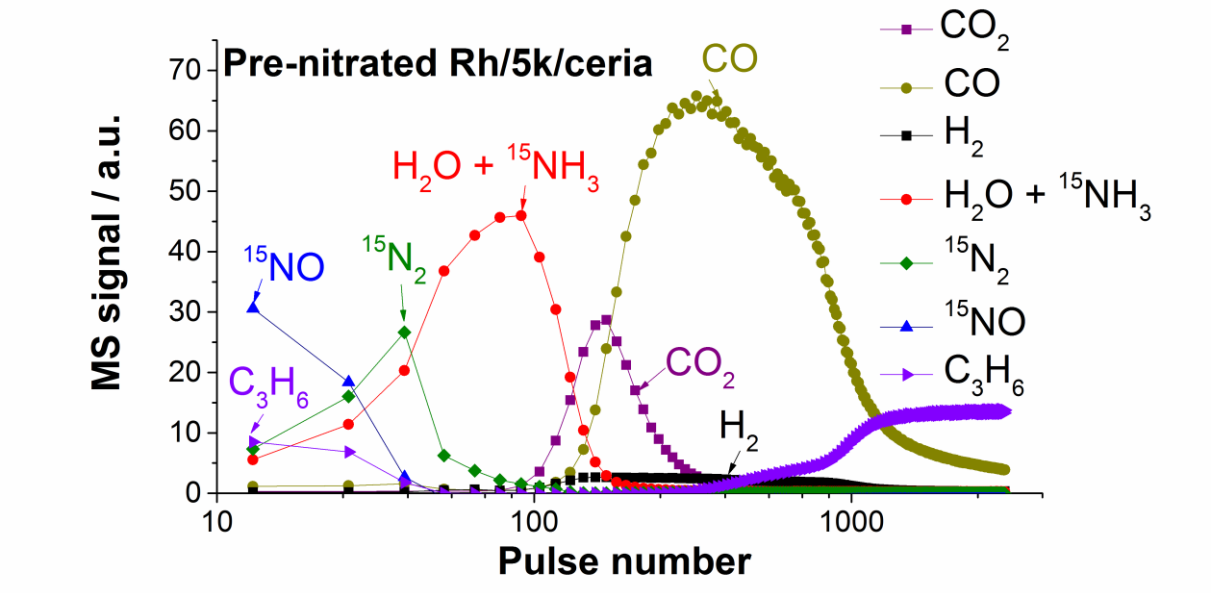

Figure 12. C_3H_6 over ^{15}NO pre-nitrated Rh/K/CZ at 450 ^{o}C, Ne was used as internal standard.

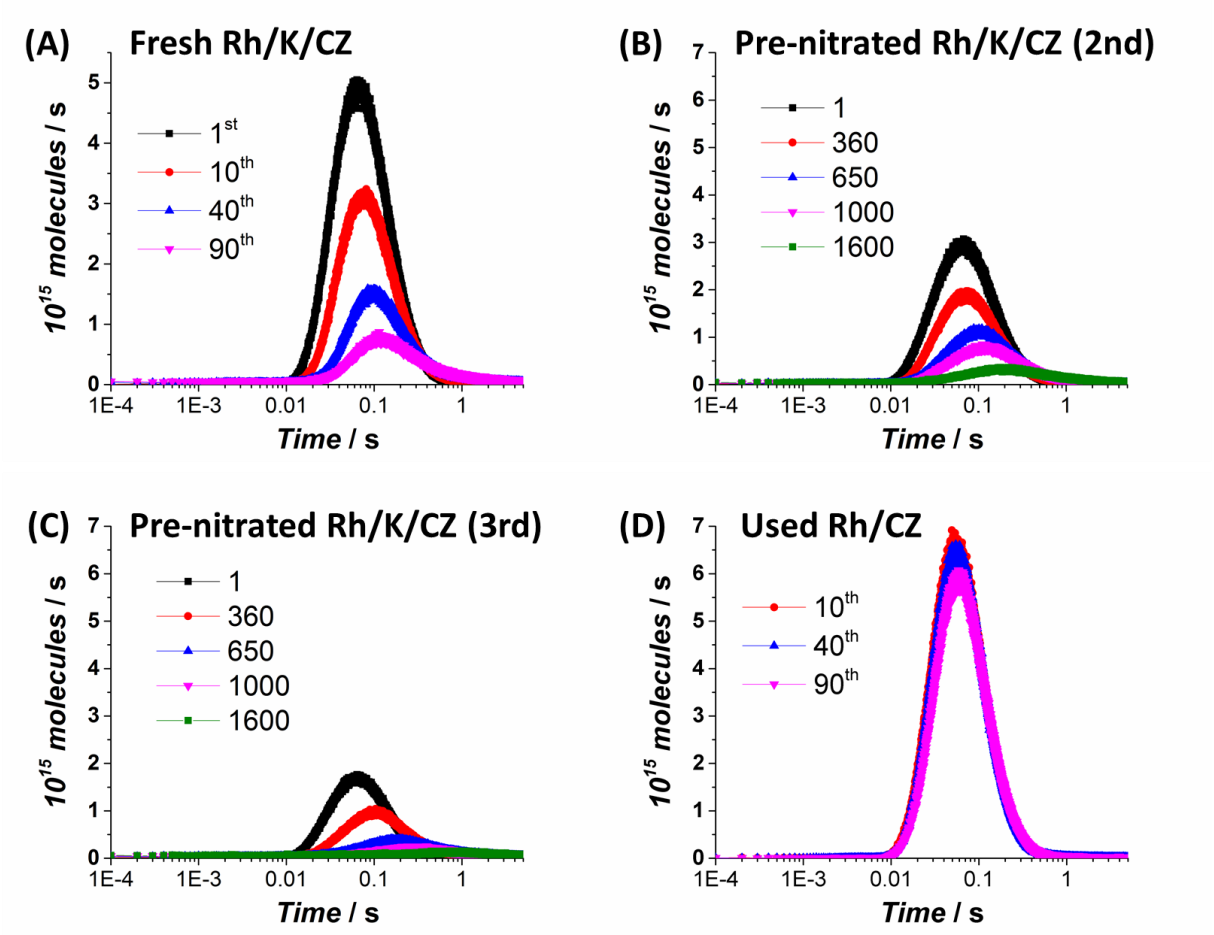

Figure 13. $^{15}N_2$ response during ^{15}NO pulses over (A) H_2 pre-reduced Rh/K/CZ (fresh), (B) C_3H_6 pre-reduced Rh/K/CZ (pre-nitrated, 2nd cycle), (C) C_3H_6 pre-reduced Rh/K/CZ (pre-nitrated, 3rd cycle), and (D) H_2 pre-reduced Rh/CZ (both used and fresh).

[1] D.C. Carslaw, S.D. Beevers, J.E. Tate, E.J. Westmoreland, M.L. Williams, Recent evidence concerning higher NOx emissions from passenger cars and light duty vehicles, Atmospheric Environment, 45 (2011) 7053-7063.
[2] L. Yang, S. Zhang, Y. Wu, Q. Chen, T. Niu, X. Huang, S. Zhang, L. Zhang, Y. Zhou, J. Hao, Evaluating real-world CO2 and NOX emissions for public transit buses using a remote wireless on-board diagnostic (OBD) approach, Environmental Pollution, 218 (2016) 453-462.
[3] F.P.S. Vicente Franco, John German, and Peter Mock, REAL-WORLD EXHAUST EMISSIONS FROM MODERN DIESEL CARS, (2014).
[4] M. Koebel, M. Elsener, T. Marti, NOx-reduction in diesel exhaust gas with urea and selective catalytic reduction, Combustion science and technology, 121 (1996) 85-102.

[5] W.R. Miller, J.T. Klein, R. Mueller, W. Doelling, J. Zuerbig, The development of urea-SCR technology for US heavy duty trucks, in, SAE Technical Paper, 2000.
[6] H. Hug, A. Mayer, A. Hartenstein, Off-highway exhaust gas after-treatment: Combining urea-SCR, oxidation catalysis and traps, in, SAE Technical Paper, 1993.
[7] S.i. Matsumoto, Recent advances in automobile exhaust catalyst, Catalysis Surveys from Asia, 1 (1997) 111-117.
[8] Y. Ikeda, K. Sobue, S. Tsuji, S.i. Matsumoto, Development of NOx Storage-Reduction Three-way Catalyst for D-4 Engines, in, SAE Technical Paper, 1999.
[9] M. Misono, T. Inui, New catalytic technologies in Japan, Catal. Today, 51 (1999) 369-375.
[10] Y. Sakamoto, T. Motohiro, S. Matsunaga, K. Okumura, T. Kayama, K. Yamazaki, T. Tanaka, Y. Kizaki, N. Takahashi, H. Shinjoh, Transient analysis of the release and reduction of NO x using a Pt/Ba/Al 2 O 3 catalyst, Catalysis Today, 121 (2007) 217-225.
[11] J. Sjöblom, K. Papadakis, D. Creaser, C.I. Odenbrand, Use of experimental design in development of a catalyst system, Catalysis today, 100 (2005) 243-248.
[12] Eu comission.
[13] Y. Bisaiji, K. Yoshida, M. Inoue, K. Umemoto, T. Fukuma, Development of Di-Air-A New Diesel deNOx System by Adsorbed Intermediate Reductants, SAE International Journal of Fuels and Lubricants, 5 (2012) 380-388.
[14] Y. Wang, M. Makkee, Fundamental understanding of the Di-Air system (an alternative NOx abatement technology):(I) the difference in reductant pre-treatment of ceria, Applied Catalysis B: Environmental, (2017).
[15] Y. Wang, J. Posthuma de Boer, F. Kapteijn, M. Makkee, Next Generation Automotive DeNOx Catalysts: Ceria What Else?, ChemCatChem, 8 (2016) 102-105.
[16] Y. Wang, R. Oord, D. van den Berg, B.M. Weckhuysen, M. Makkee, Oxygen Vacancies in Reduced Rh/ and Pt/Ceria for Highly Selective and Reactive Reduction of NO into N2 in excess of O2, ChemCatChem, 9 (2017) 2935-2938.
[17] Y. Wang, F. Kapteijn, M. Makkee, NOx reduction in the Di-Air system over noble metal promoted ceria, Applied Catalysis B: Environmental, 231 (2018) 200-212.
[18] W.S. Epling, L.E. Campbell, A. Yezerets, N.W. Currier, J.E. Parks, Overview of the fundamental reactions and degradation mechanisms of NOx storage/reduction catalysts, Catalysis Reviews, 46 (2004) 163-245.
[19] N. Takahashi, K. Yamazaki, H. Sobukawa, H. Shinjoh, The low-temperature performance of NO x storage and reduction catalyst, Applied Catalysis B: Environmental, 70 (2007) 198-204.
[20] W.S. Epling, A. Yezerets, N.W. Currier, The effects of regeneration conditions on NO x and NH 3 release from NO x storage/reduction catalysts, Applied Catalysis B: Environmental, 74 (2007) 117-129.
[21] Y. Wang, J.P. Boer, F. Kapteijn, M. Makkee, Fundamental Understanding of the Di-Air System: The Role of Ceria in NO x Abatement, Topics in Catalysis, 1-7.
[22] H.C. Yao, Y.F.Y. Yao, Ceria in automotive exhaust catalysts: I. Oxygen storage, Journal of Catalysis, 86 (1984) 254-265.
[23] M. Daturi, E. Finocchio, C. Binet, J.-C. Lavalley, F. Fally, V. Perrichon, H. Vidal, N. Hickey, J. Kašpar, Reduction of High Surface Area CeO2−ZrO2 Mixed Oxides, The Journal of Physical Chemistry B, 104 (2000) 9186-9194.
[24] C.M. Kalamaras, G.G. Olympiou, V.I. Pârvulescu, B. Cojocaru, A.M. Efstathiou, Selective catalytic reduction of NO by H2/C3H6 over Pt/Ce1-xZrxO2-δ: The synergy effect studied by transient techniques, Applied Catalysis B: Environmental, 206 (2017) 308-318.
[25] G.N. Vayssilov, M. Mihaylov, P.S. Petkov, K.I. Hadjiivanov, K.M. Neyman, Reassignment of the vibrational spectra of carbonates, formates, and related surface species on ceria: a combined density functional and infrared spectroscopy investigation, The Journal of Physical Chemistry C, 115 (2011) 23435-23454.
[26] V. Matsouka, M. Konsolakis, R.M. Lambert, I.V. Yentekakis, In situ DRIFTS study of the effect of structure (CeO2–La2O3) and surface (Na) modifiers on the catalytic and surface behaviour of Pt/γ-

Al2O3 catalyst under simulated exhaust conditions, Applied Catalysis B: Environmental, 84 (2008) 715-722.
[27] N. Bion, J. Saussey, M. Haneda, M. Daturi, Study by in situ FTIR spectroscopy of the SCR of NOx by ethanol on Ag/Al2O3—Evidence of the role of isocyanate species, Journal of Catalysis, 217 (2003) 47-58.
[28] N. Hou, Y. Zhang, M. Meng, Carbonate-based lean-burn NOx trap catalysts Pt–K2CO3/ZrO2 with large NOx storage capacity and high reduction efficiency, The Journal of Physical Chemistry C, 117 (2013) 4089-4097.
[29] A. Iordan, M.I. Zaki, C. Kappenstein, C. Géron, XPS and in situ IR spectroscopic studies of CO/Rh/Al 2 O 3 and CO/Rh/K–Al 2 O 3 at high temperatures: probing the impact of the potassium functionalization of the support, Physical Chemistry Chemical Physics, 5 (2003) 1708-1715.
[30] Z.-Q. Zou, M. Meng, J.-J. He, Surface distribution state and storage performance of the potassium species in the lean-burn NOx trap catalyst Pt/K/Al2O3–TiO2–ZrO2, Materials Chemistry and Physics, 124 (2010) 987-993.
[31] I. Nova, L. Castoldi, L. Lietti, E. Tronconi, P. Forzatti, F. Prinetto, G. Ghiotti, NOx adsorption study over Pt–Ba/alumina catalysts: FT-IR and pulse experiments, Journal of Catalysis, 222 (2004) 377-388.
[32] Y. Peng, J. Li, X. Huang, X. Li, W. Su, X. Sun, D. Wang, J. Hao, Deactivation Mechanism of Potassium on the V2O5/CeO2 Catalysts for SCR Reaction: Acidity, Reducibility and Adsorbed-NOx, Environmental Science & Technology, 48 (2014) 4515-4520.
[33] M. Symalla, A. Drochner, H. Vogel, S. Philipp, U. Göbel, W. Müller, IR-study of formation of nitrite and nitrate during NO x-adsorption on NSR-catalysts-compounds CeO 2 and BaO/CeO 2, Topics in Catalysis, 42 (2007) 199-202.
[34] T. Montanari, L. Castoldi, L. Lietti, G. Busca, Basic catalysis and catalysis assisted by basicity: FT-IR and TPD characterization of potassium-doped alumina, Applied Catalysis A: General, 400 (2011) 61-69.
[35] K. Krishna, A. Bueno-López, M. Makkee, J. Moulijn, Potential rare-earth modified CeO 2 catalysts for soot oxidation part II: Characterisation and catalytic activity with NO+ O 2, Applied Catalysis B: Environmental, 75 (2007) 201-209.
[36] S. Mulla, S. Chaugule, A. Yezerets, N. Currier, W. Delgass, F. Ribeiro, Regeneration mechanism of Pt/BaO/Al 2 O 3 lean NO x trap catalyst with H 2, Catalysis Today, 136 (2008) 136-145.
[37] F. Can, X. Courtois, S. Royer, G. Blanchard, S. Rousseau, D. Duprez, An overview of the production and use of ammonia in NSR+ SCR coupled system for NO x reduction from lean exhaust gas, Catalysis today, 197 (2012) 144-154.
[38] A. Kouakou, F. Dhainaut, P. Granger, F. Fresnet, I. Louis-Rose, Study of Ammonia Formation During the Purge of a Lean NO x Trap, Topics in Catalysis, 52 (2009) 1734.
[39] B.K. Cho, B.H. Shank, J.E. Bailey, Kinetics of NO reduction by CO over supported rhodium catalysts: Isotopic cycling experiments, Journal of Catalysis, 115 (1989) 486-499.
[40] F. Fajardie, J.-F. Tempère, J.-M. Manoli, O. Touret, G. Blanchard, G. Djéga-Mariadassou, Activity of Rhx+ Species in CO Oxidation and NO Reduction in a CO/NO/O2Stoichiometric Mixture over a Rh/CeO2-ZrO2Catalyst, Journal of Catalysis, 179 (1998) 469-476.